Journal of Volcanology and Geothermal Research 414 (2021) 107229

Contents lists available at ScienceDirect

Journal of Volcanology and Geothermal Research

journal homepage: www.elsevier.com/locate/jvolgeores

Invited Research Article

A microanalytical oxygen isotopic and U-Th geochronologic investigation and modeling of rhyolite petrogenesis at the Krafla Central Volcano, Iceland

Hampton R.L. [a,*], I.N. Bindeman [a,b], R.A. Stern [c], M.A. Coble [d,e], S.M. Rooyakkers [f]

[a] Department of Earth Sciences, 1272 University of Oregon, Eugene, OR 97403-1272, United States of America
[b] Fersman Mineralogical Museum, Moscow, Russia
[c] Canadian Centre for Isotopic Microanalysis, Department of Earth and Atmospheric Sciences, University of Alberta, Edmonton, AB T6G 2R3, Canada
[d] Stanford-USGS Ion Microprobe Laboratory, Stanford University, 450 Serra Mall, Stanford, California 94305, United States of America
[e] School of Geography, Environment and Earth Sciences, Victoria University of Wellington, Wellington 6140, New Zealand
[f] Department of Earth and Planetary Sciences, 3450 University Street, McGill University, Montreal, Quebec, Canada

ARTICLE INFO

Article history:
Received 7 July 2020
Received in revised form 24 February 2021
Accepted 8 March 2021
Available online 17 March 2021

Keywords:
Oxygen isotope
Rhyolite petrogenesis
Krafla
Assimilation
Fractional crystallization
Zircon

ABSTRACT

Understanding the petrogenesis of silicic magmas is critical for understanding the volcanic hazards they pose, their geothermal energy potential, and the creation of continental crust. In this study we explore the origin of rhyolitic magmas in basaltic crust at the Krafla Central Volcano in Iceland. We present laser fluorination oxygen isotope analyses of plagioclase, pyroxene, and groundmass from eight rhyolites and six selected basalts, as well as in situ oxygen isotope analyses and U-Th geochronology of zircons from three rhyolitic domes erupted around the caldera margins. Zircon U-Th geochronology for the rhyolite domes yields ages of 88.7 ± 9.9 ka for Jörundur, 83.3 ± 9.2 ka for Hlíðarfjall, and 85.5 ± 9.4 ka for Gæsafjallarani, some 20–30 ka after the eruption of the zoned rhyolite to basalt Halarauður ignimbrite during a major collapse of the Krafla caldera. We suggest that the domes represent a renewed episode of silicic magma production in the pre-heated crust. Oxygen isotope analyses of single and bulk plagioclase and pyroxene identify some instances of isotopic disequilibrium with groundmass (~3.5‰) reflecting assimilation of diverse low $\delta^{18}O$ crustal material. However, zircon is largely in equilibrium with groundmass analyses, suggesting it crystallized directly from low $\delta^{18}O$ magma. Zircon trace elements (Hf, Yb, Th, U) for all three domes show trends indicative of fractional crystallization. Pairing these observations with two-dimensional thermal modeling using the Heat2D model, and chemical modeling using the Magma Chamber Simulator, we suggest that petrogenesis of rhyolitic magma at Krafla requires at least two-steps: the $\delta^{18}O$ of basaltic parental magmas are first lowered through assimilation of hydrothermally altered material (generated in the high temperature region in the crust surrounding the magma chamber) to produce low $\delta^{18}O$ mafic to intermediate magmas, which then ascend from magma generation zones into colder crust where they undergo further fractional crystallization at shallower depths. Our models suggest that prior hydrothermal alteration of the mafic crust greatly increases the volume of partial melt that can be produced and assimilated, and we thus suggest that long-lived hydrothermal systems may play an important role in further encouraging the production of larger volumes of rhyolitic magmas in basalt-dominated environments.

1. Introduction

Seated at the intersection of a subaerial mid-ocean ridge and upwelling mantle plume, Iceland is a natural laboratory for studying silicic magma generation in basalt-dominated extensional environments (Bindeman et al., 2012; Carley et al., 2020; Carley et al., 2014; Jónasson, 2007; Jónasson, 1994; Martin and Sigmarsson, 2010; Pope et al., 2013; Schattel et al., 2014). The Icelandic crust is dominantly basaltic, but also hosts up to 15% silicic intrusive and extrusive rocks (Maas et al., 1992; Marsh et al., 1991; Martin et al., 2008). This greater occurrence of silicic magmatism and volcanism in a basalt-dominated setting has important implications; Iceland's silicic magmas present eruption hazards that can affect both Iceland and mainland Europe, but also provide a long-lived heat source for hydrothermal power, and may provide a modern analog for the generation of continental crust in early Earth-like environments (Bindeman et al., 2012; Maas et al., 1992; Marsh et al., 1991; Martin et al., 2008; Reimink et al., 2014).

* Corresponding author.
E-mail address: rhampton@uoregon.edu (R.L. Hampton).

https://doi.org/10.1016/j.jvolgeores.2021.107229
0377-0273/

Despite these implications and decades of scientific interest, the petrogenesis of silicic magmas in Iceland and other predominantly basaltic settings remains highly debated.

Many rocks in Iceland, including many of the erupted rhyolites and much of the crust that has been explored via drilling, are characterized by low $\delta^{18}O$ isotopic compositions. Crustal $\delta^{18}O$ values are on average ~ 1–3‰ lower than normal mantle values in the Icelandic rift zones (Gautason and Muehlenbachs, 1998), and reach much lower values in areas of extensive hydrothermal alteration; altered rocks from Krafla boreholes have bulk $\delta^{18}O$ as low as −12‰ (average upper crustal value = −7.7 ± 2.4‰; Hattori and Muehlenbachs, 1982). This strong isotopic contrast between the Icelandic crust and mantle-derived magmas provides a useful tool to constrain the role of magmatic-crustal interactions in Iceland, and is particularly useful in probing the origins of the silicic magmas, which mainly occur around the central volcanoes where large hydrothermal systems are located (Hattori and Muehlenbachs, 1982; Nicholson et al., 1991; Pope et al., 2013). While it has been hypothesized that moderately low $\delta^{18}O$ magmas originate from an anomalously low $\delta^{18}O$ component of the Icelandic mantle or plume (Maclennan et al., 2002; Winpenny and Maclennan, 2014), the values observed in volcanic rocks at Krafla are too low and variable to reflect such an anomaly alone, and must reflect interaction between crustal rocks and meteoric water in some fashion (Bindeman et al., 2012; Bindeman et al., 2008; Eichelberger, 2020; Eichelberger et al., 2020).

Zircons, though not always present in Icelandic rhyolites, provide an additional tool for understanding silicic magma petrogenesis and, in particular, the origins of the low $\delta^{18}O$ magmas in Iceland (Banik et al., 2018; Bindeman et al., 2012; Bindeman and Melnik, 2016; Carley et al., 2020; Carley et al., 2014; Carley et al., 2011; Gurenko et al., 2015; Reimink et al., 2014). Because of their high closure temperature, zircon grains hold a robust record of the $\delta^{18}O$ signature imprinted on them during crystallization (Carley et al., 2020; Gurenko et al., 2015; Valley et al., 1994; Watson and Harrison, 1983). Crystal size distributions, and trace element analyses further increase the utility of detailed zircon investigation.

In this study, we utilize detailed zircon analyses, including oxygen isotope measurements, U-Th dating, trace element, and crystal size distribution analysis, to gain insights on the petrogenesis of rhyolite at Krafla volcano in the Northern Volcanic Zone of Iceland. We combine this zircon work with laser-fluorination $\delta^{18}O$ analysis of plagioclase, clinopyroxene and host groundmass from Krafla volcanic products ranging in composition from basalt to rhyolite. These data are then paired with thermal and chemical modeling to explore the relative importance of fractional crystallization versus partial melting and assimilation processes in the generation of Krafla rhyolites. We conclude by proposing a new conceptual model for the petrogenesis of the rhyolites at Krafla, consistent with thermal, chemical, and isotopic constraints, that reconciles the previous controversy surrounding their origin and may also be applicable in other Icelandic systems.

1.1. Geology of Krafla

The Krafla volcanic system consists of a central volcano, hosting a ~ 8 × 10 km ellipsoidal caldera, which is bisected by a 100 km-long fissure system (Sæmundsson, 1991; Jónasson, 1994). This system is ideal for investigating the production of rhyolite in a basaltic environment for several reasons. First, Krafla has a ca. 240 kyr record of concurrent silicic and mafic volcanism (based on $^{40}Ar/^{39}Ar$ dating of a dacite recognized as its oldest silicic product; Sæmundsson and Pringle, 2000), providing an opportunity to study a variety of rhyolites and their relationship with temporally- and spatially-related basaltic magmas (Jónasson, 1994; Nicholson et al., 1991; Sæmundsson, 1991). Second, Krafla hosts a large hydrothermal system where meteoric water, isotopically depleted to values between −10 and − 13‰ due to the high latitudes and cold climate of Iceland, has infiltrated the heated crust (Gautason and Muehlenbachs, 1998; Hattori and Muehlenbachs, 1982; Pope et al., 2014; Pope et al., 2013; Zakharov et al., 2019). This has resulted in extensive hydrothermal alteration of the crust to isotopically depleted (low $\delta^{18}O$) values (−3 to −12‰) (Eichelberger et al., 2020; Hattori and Muehlenbachs, 1982; Pope et al., 2013) that are in significant contrast to the mantle-derived basalts (+5.5‰) that feed the magmatic system. This contrast provides excellent leverage to study the interactions between the intruding magmas and surrounding mafic crust, which are otherwise compositionally similar (Bindeman, 2008; Hattori and Muehlenbachs, 1982; Pope et al., 2014; Sveinbjornsdóttir et al., 2015).

Rhyolitic activity at Krafla was divided into three phases by Jónasson (1994) (Figs. 1, 2, and 3). The first, phase 1, involved emplacement of a small, poorly exposed rhyolite dome near the southern margin of the Hágöng plateau at 190 ka, and subsequent eruption of the mixed basalt-rhyolite Halarauður ignimbrite at ca. 110–115 ka ($^{40}Ar/^{39}Ar$ dates from Sæmundsson and Pringle, 2000; Figs. 1 and 3D). The Halarauður eruption is the largest known eruption of Krafla (total 7 ± 6 km^3 of magma) and was linked with major caldera collapse (Calderone et al., 1990; Rooyakkers et al., 2020). Phase 2 occurred during the last glacial period and involved the emplacement of three subglacial rhyolite domes around the caldera margin. These domes, with a cumulative volume of ~0.7 km^3, are believed to have exploited caldera ring fractures. From the southeast clockwise to the northwest they are Jörundur, Hlíðarfjall, and Gæsafjallarani (Figs. 1 and 2). Previous $^{40}Ar/^{39}Ar$ geochronology provides age constraints for Jörundur and Gæsafjallarani of 85–90 ka and 83–85 ka, respectively (Sæmundsson and Pringle, 2000). Phase 3 began at ca. 24 ka with the subglacial rhyolite fissure eruption (volume < 0.05 km^3) that formed the obsidian ridge, Hrafntinnuhryggur, in the southeast section of the caldera (Jónasson, 1994; Tuffen and Castro, 2009) (Figs. 1 and 3A, B, C). This was followed by eruption of the 9 ka Hveragil Tephra in the central region of the caldera (not part of this study), and a small phreatomagmatic eruption in 1724 CE at the onset of the Mývatn Fires rifting episode, which formed Víti crater (Fig. 3E). The Víti eruption ejected scarce juvenile rhyolitic pumice and basaltic scoria, and xenolith blocks of granophyre and felsite (Grönvold, 1984; Jónasson, 1994; Thorarinsson, 1979) (Fig. 3E). Episodic outpouring of large basaltic lava flows continued from fissures to the west until 1729 (Grönvold, 1984). The most recent eruptions at Krafla occurred during the 1975–1984 Krafla Fires rifting episode and were exclusively basaltic. Numerous other effusive basaltic eruptions at Krafla occurred throughout the Holocene (Sæmundsson, 1991; Thorarinsson, 1979).

In 2009, IDDP-1, the first well of the International Deep Drilling Project, drilled into the Krafla hydrothermal system and unintentionally intersected near liquidus (~930 °C) rhyolite magma at 2.1 km depth (Elders et al., 2014; Elders et al., 2011; Zierenberg et al., 2013) (Fig. 1). The transition during drilling from the ~300 °C hydrothermal regime to ~930 °C occurred over ~30 m (Eichelberger, 2020). Triple oxygen isotope data suggest that this low $\delta^{18}O$ (+3.1‰) rhyolite was formed predominantly by assimilation of partial melts from hydrothermally altered and isotopically depleted basaltic crust into intruding basaltic magma (Zakharov et al., 2019), with altering waters tracing back to the last glacial (Pope et al., 2014; Zakharov et al., 2019). This magma provides a rare glimpse into the active upper crustal petrogenetic factory (Eichelberger et al., 2020).

1.2. Previous models for rhyolite petrogenesis at Krafla

Previous petrologic and geochemical studies at Krafla have resulted in two endmember models to explain the petrogenesis of its high-silica, low $\delta^{18}O$ rhyolites (Fig. 4):

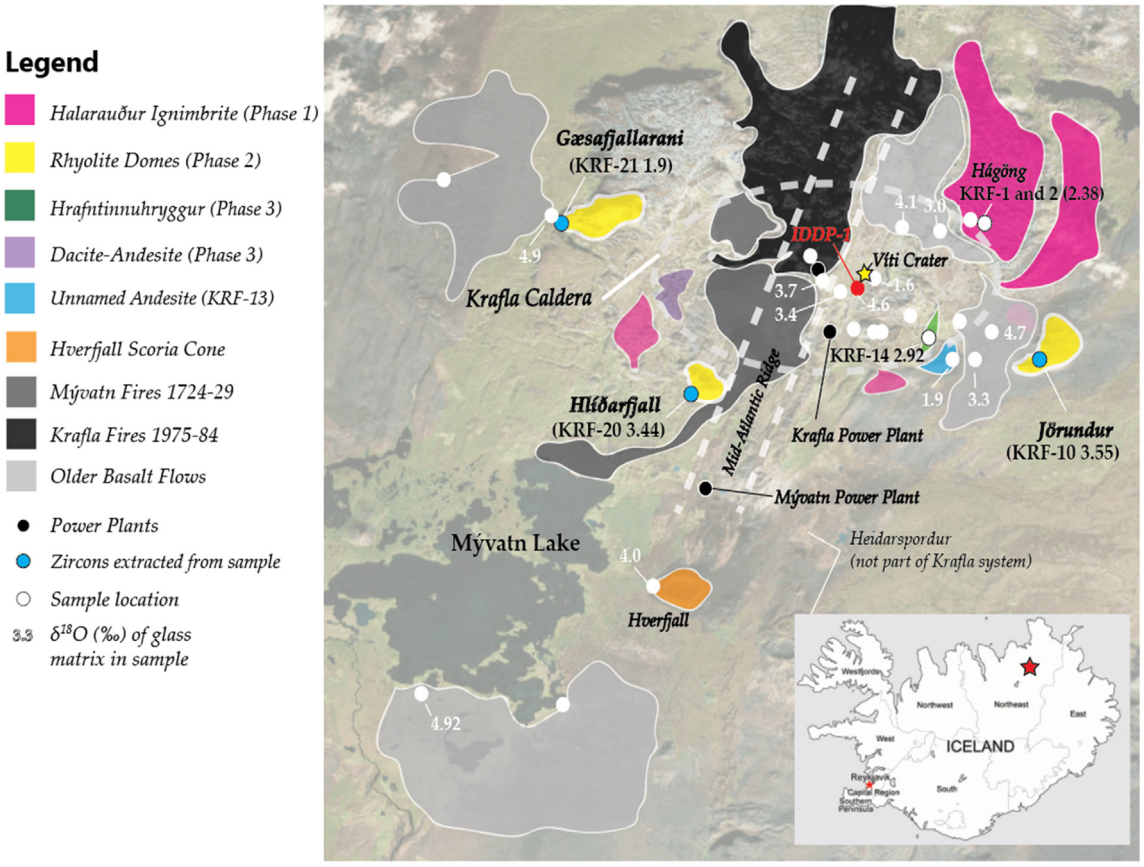

Fig. 1. Map of Krafla. Simplified map of the Krafla central volcano and caldera, highlighting the units sampled in this study (modified from Jónasson, 1994). The outset map shows the location of the Krafla central volcano (red star) in the northeast of Iceland along the Northern Volcanic Zone. (For interpretation of the references to colour in this figure legend, the reader is referred to the web version of this article.)

1) A classic assimilation and fractional crystallization (AFC) model where the latent heat released during fractional crystallization (FC) of a basaltic magma chamber induces assimilation of partially melted (or bulk) basaltic crust surrounding the chamber (Fig. 4B) (Charreteur et al., 2013; Nicholson et al., 1991).
2) A model involving predominantly crustal melting, where partial melt is formed in the heated zone around an intruded basaltic magma chamber and segregates to form its own magma body without interacting with (i.e., mixing or assimilating into) the basaltic magma (Fig. 4A) (Jónasson, 1994; Zierenberg et al., 2013).

Whole rock chemical trends that follow fractional crystallization patterns, supported by mass balance calculations, have been used as the central evidence for identifying FC processes at Krafla and other silicic systems in Iceland (Carmichael, 1964; Furman et al., 1992; Hards et al., 2000; Kokfelt et al., 2009; Macdonald et al., 1990; Nicholson et al., 1991). However, Nicholson et al. (1991) noted that isotopic compositions (especially O- and U- series isotopes) of Krafla's silicic rocks required some contribution from low $\delta^{18}O$ and older (at Th-U equiline) crust. They thus devised an AFC model for the generation of Krafla rhyolites; fractional crystallization was believed to be primarily responsible for differentiating the magmas, while the latent heat of crystallization drove the assimilation of partial melt from hydrothermally altered wallrock to produce their low $\delta^{18}O$ isotopic signature.

The second model for differentiation at Krafla suggests that low-degree (5–15%), high-silica partial melt is formed in the heated wallrock zone around upper-crustal basaltic magma chambers and segregates away from the melting zone through cracks and melt channels to form rhyolitic magma bodies (Jónasson, 1994; Fig. 4A). This model was based primarily on similarities between the major element chemistries of the rhyolites and experimental melts of altered basaltic rocks at low pressure and low P_{H2O}, as well as their low $\delta^{18}O$ compositions and the scarcity of intermediate magmas erupted at Krafla (Jónasson, 2007; Jónasson, 1994).

This paper contributes new data and aims to resolve these conflicting models for the generation of rhyolites at Krafla and other basalt-dominated settings. The objective of this study is to combine the existing petrologic knowledge for Krafla with detailed isotopic analysis of zircon crystal populations with thermochemical modeling, and to quantify via heat, mass, and isotope balances the relative importance of FC, assimilation and partial melting of altered crust in producing Krafla rhyolites.

2. Methods

For full details on all methods see the Supplementary Material.

2.1. Analytical methods

Samples were collected from the following units (Figs. 1–3): 1) the ~190 ka pre-caldera rhyolite dome at the southern edge of Hágöng, 2) the ~110–115 ka Halarauður ignimbrite (units H2 and H3 of Rooyakkers et al., 2020), 3) the three post-caldera rhyolite domes, Jörundur, Gæsafjallarani and Hlíðarfjall, 4) the ~24 ka obsidian ridge Hraftntinnuhryggur, and 5) the 1724 CE Víti crater pumice and felsite xenoliths. Samples of quenched glass from the rhyolitic magma encountered in the IDDP-1 well in 2009 were also acquired. Several basaltic lavas from recent fissure eruptions were also sampled around the caldera (Fig. 1).

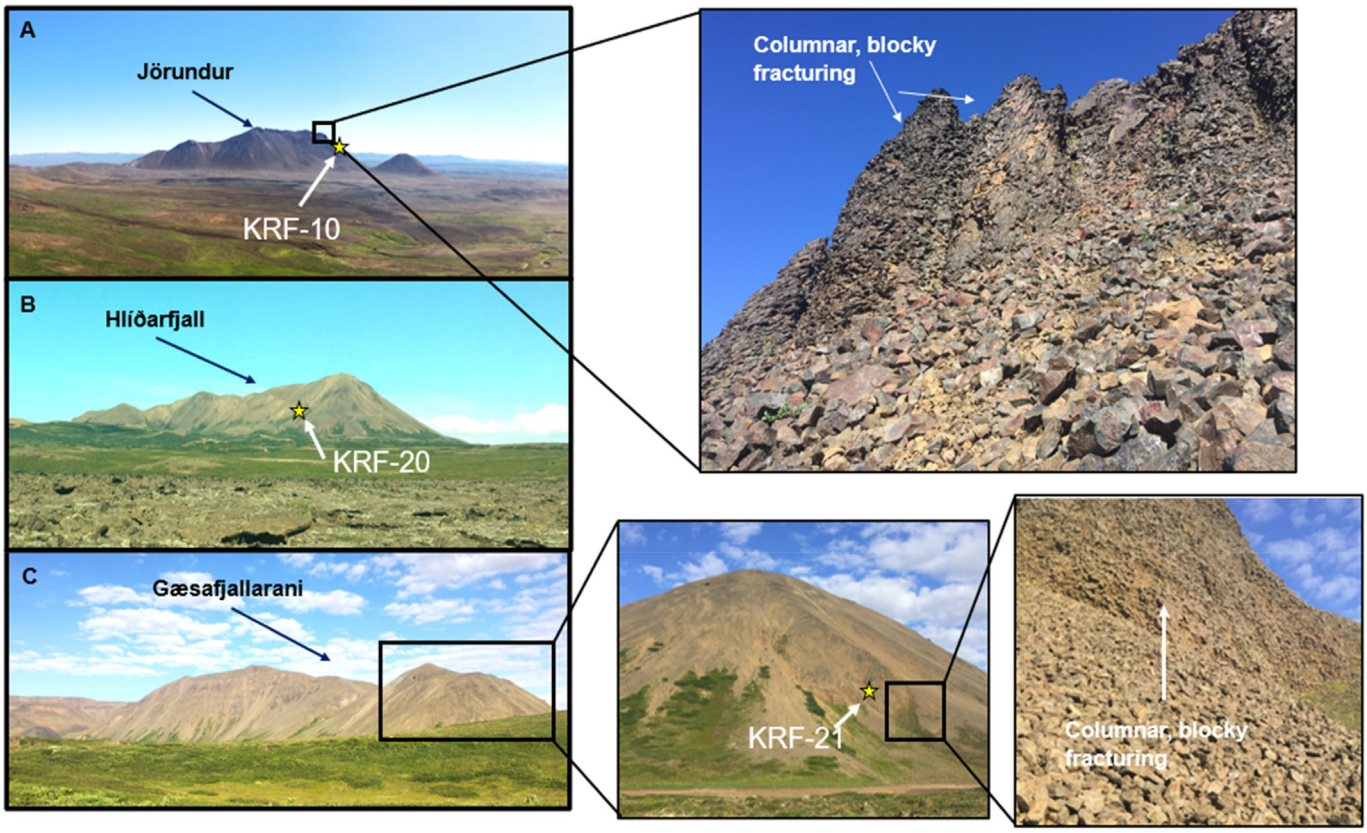

Fig. 2. The Phase 2 Rhyolite Domes. A) Jörundur, located SE of the caldera margin (see Fig. 1 for dome locations), with basaltic lava flows from the fissure system in the foreground. Outset shows columnar jointing and blocky fracturing patterns formed during subglacial emplacement. Some localities along the base of the dome show glassy textures. B) Hlíðarfjall, located SW of the caldera margin. C) Gæsafjallarani with outsets showing sample location of KRF-21 and blocky columnar jointing. All samples from these domes yielded zircons.

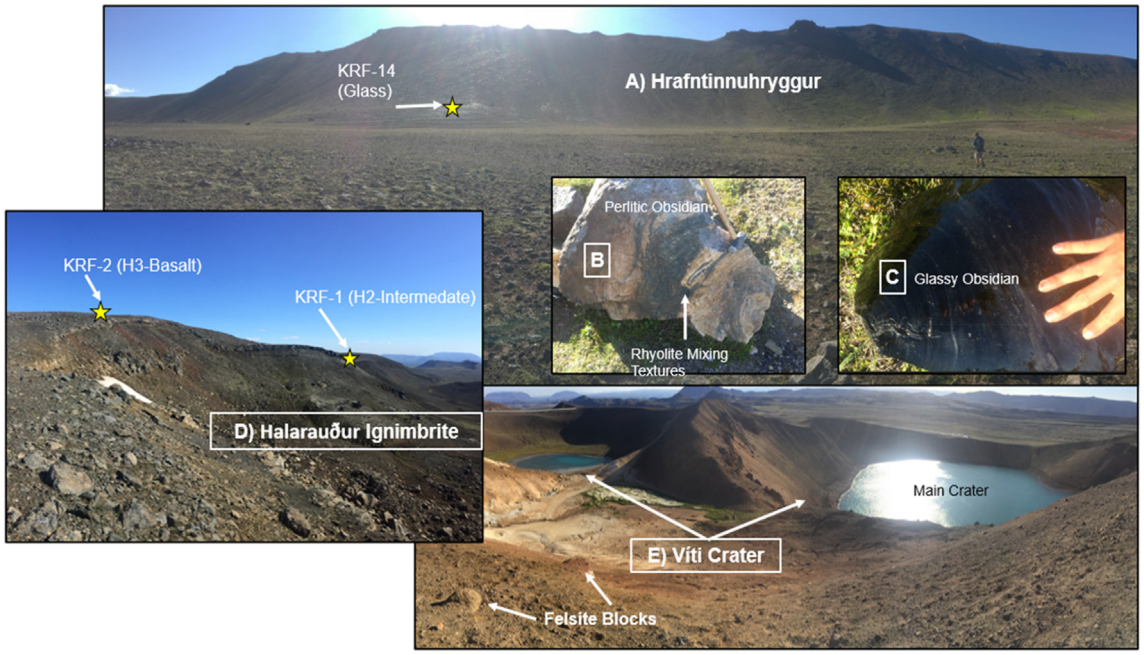

Fig. 3. Selected Units Sampled. A) Obsidian ridge (Hrafntinnuhryggur). Two central textures are present across the ridge, B) a perlitic texture as well as C) a glassy texture. D) Ridge composed of the Halarauður ignimbrite, erupted during a major caldera collapse event. At both sample locations the tuff has a high volume of lithic fragments and sparse crystals. E) Vití crater, the site of Krafla's youngest rhyolitic eruption.

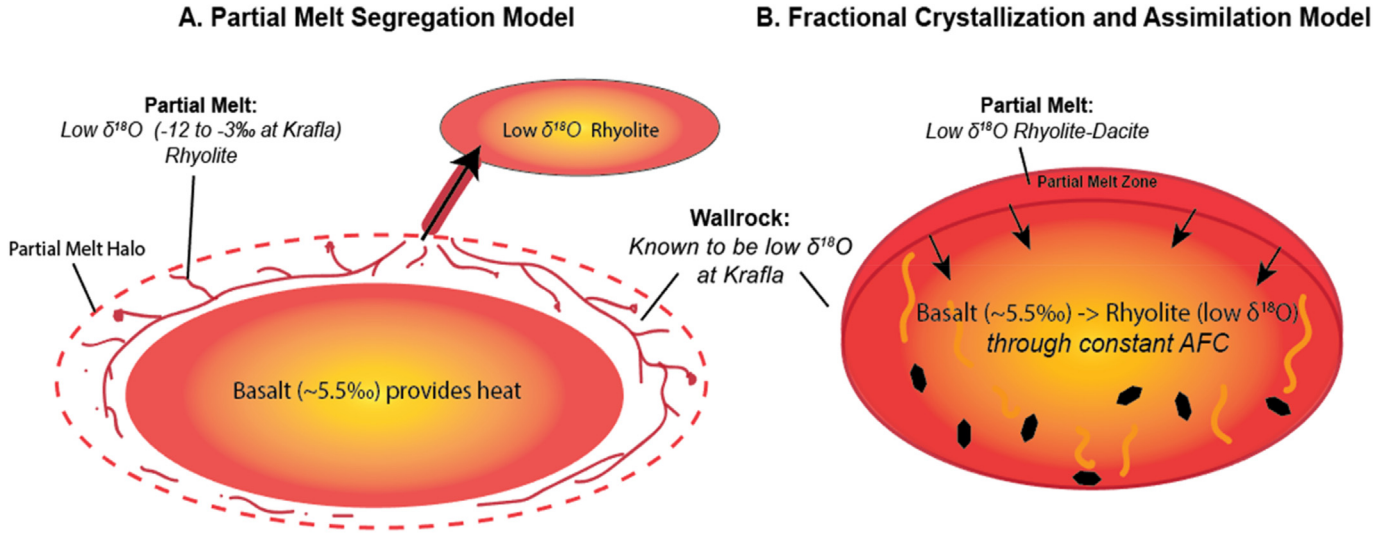

Fig. 4. Previous Models for Rhyolite Petrogenesis at Krafla. Schematic representations of previous hypotheses for rhyolite production at Krafla. A) Model dominated by segregation of partial melt (Jónasson, 1994). Rhyolitic, low $\delta^{18}O$ partial melt forms around the margins of large basaltic magma bodies. This partial melt segregates through cracks and melt channels to form rhyolitic magma bodies. B) Model dominated by fractional crystallization and simultaneous assimilation (AFC) (Nicholson et al., 1991; Charreteur et al., 2013). Partial melting of the low $\delta^{18}O$ hydrothermally altered wallrock is induced by the intrusion and crystallization of basaltic magma and assimilated into the fractionating and magma chamber; alternatively, bulk crust may be assimilated by stoping.

Zircon separation by standard and HF-extraction techniques were performed on all units sampled, but yielded zircons only in the three rhyolitic ring fracture domes. Zircons extracted from these samples were mounted in epoxy resin, polished, and imaged by cathodoluminescence (CL) (Fig. 5, Supplement Fig.A). The mounted zircons were then analyzed for oxygen isotopes by SIMS at the University of Alberta using a 15 μm-diameter Cs^+ beam (Fig. 5). Following O isotope analyses, analytical pits (depths of ~1 μm) were polished away, and the same crystals spots were then targeted by O_2^- beam for ^{238}U-^{230}Th-^{232}Th isotopes and select trace element concentrations (U, Th, Hf, Yb) by using the SHRIMP-RG SIMS at Stanford University, following methods similar to Coble et al. (2018) and Mucek et al. (2017). This approach enabled direct comparison of individual $\delta^{18}O$ values, ages and elemental ratios for the same analytical spots. Isochron ages were calculated using whole rock U/Th ratios measured by solution ICP-MS (Rooyakkers et al., 2021; Rooyakkers, 2020) to estimate the host rock U-Th activity ratio: Jörundur $^{238}U/^{232}Th = 0.3068 \pm 0.01$, Hlíðarfjall $^{238}U/^{232}Th = 0.3059 \pm 0.01$, and Gæsafjallarani $^{238}U/^{232}Th = 0.3051 \pm 0.01$. The model assumes secular equilibrium (i.e., the $^{238}U/^{232}Th$ activity ratio is equal to the $^{230}Th/^{232}Th$ activity ratio). In the absence of isotope dilution U and

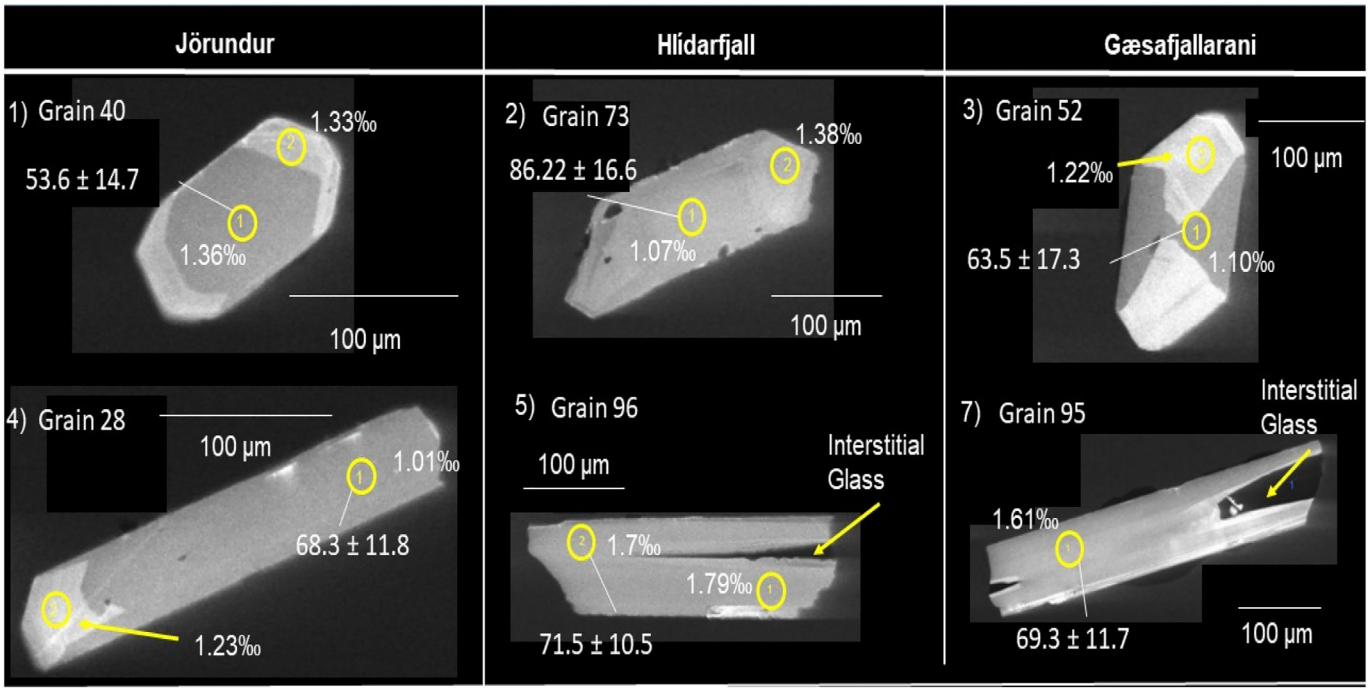

Fig. 5. Zircon Cathodoluminescence Images. Zircons from the post-caldera domes imaged by cathodoluminescence (CL) show two morphologies: 1) an equant sector zoned morphology and 2) an elongated, splintered morphology. An example of each type is shown here for each dome.

Th ratios of glass, these ICP-MS measurements are inferred to be the most accurate proxies to use in the age model.

Zircon crystal size distribution analysis (CSD) was performed following Simakin and Bindeman (2008 and references therein), applying theoretical considerations derived by Marsh (2007, 1988). As shown by Simakin and Bindeman (2008), the zircon extraction process preserves the smallest size fraction (>10–20 um) and does not introduce a size bias into the size distribution.

Phenocrysts (if present) and groundmass $\delta^{18}O$ analyses were conducted by CO_2 laser fluorination at the University of Oregon on a MAT 253 isotope ratio mass spectrometer (Bindeman, 2008). Select units were also analyzed for whole rock major and trace element concentration by X-ray fluorescence (XRF) at Pomona University.

2.2. Thermal and chemical modeling

Chemical and thermal modeling was applied to constrain the likely thermal structure of the crust and the corresponding processes involved in producing low $\delta^{18}O$ Krafla rhyolites. We first used the Heat 2D thermal model (Annen, 2009; Annen and Sparks, 2002), to establish the thermal conditions expected in the upper crust at Krafla and to constrain where partial melting could occur. The resulting thermal constraints were then combined with the chemical and mass balance model of the Magma Chamber Simulator (MCS) to understand how the oxygen isotope and whole rock chemistry might vary during the partial melting and assimilation of different crustal compositions (Bohrson et al., 2014; Bohrson and Spera, 2001; Ghiorso and Sack, 1995).

Initial and boundary conditions for these models were derived from a variety of data sources gathered at Krafla (Supplement Table 1). Initial temperatures, whole rock chemistries, and isotopic compositions of intruding basalts were assumed from published chemical and isotopic data from Krafla, which suggest whole-rock $\delta^{18}O$ values of ~ + 5.0‰ (only slightly lower than normal mantle values) and temperatures between 1000 and 1200 °C for the basaltic magmas feeding into the main fissure system (Cooper et al., 2016; Nicholson, 1990; Nicholson and Latin, 1992; Sigmarsson and Steinthórsson, 2007; Thorarinsson, 1979). Modeled wallrock compositions and $\delta^{18}O$ values were derived from drillhole data collected from Krafla geothermal wells (Elders et al., 2014; Hattori and Muehlenbachs, 1982; Pope et al., 2014) as well as other published compositions (Kuo, 2017; Spulber and Rutherford, 1982; Wolf and Wyllie, 1995). Our new zircon geochronological data provides further constraint on the timescales involved in generating the dome magmas. These input parameters are summarized in Supplementary Table 1.

Next, the initial conditions were modified from a simple geothermal gradient of 30 °C/km (representative of crust outside the active rift zones of Iceland; (Martin and Sigmarsson, 2007)) by a 500 kyr period of crustal "priming", in which basaltic intrusions of 50 m thickness were injected every 5–10 thousand years. The assumed 500 kyr duration of priming is broadly consistent with the lifespan of the Krafla system (at least 300 ka; Sæmundsson, 1991) and accounts for the establishment and thermal maturation of the incipient magmatic system. The priming results in a steep shallow-crustal geotherm (Fig. 11A), which was then used as the input temperature conditions for subsequent runs to model melt production. The geothermal gradient produced by this priming run is consistent with well data from Krafla (Axelsson et al., 2014).

Following initial thermal priming, sills were emplaced every 500 years during the subsequent 50 kyr at random depths between 3.5 and 5 km. The 500 year interval between intrusions is consistent with the frequency of major rifting events on the Krafla fissure swarm (one event every 300–1000 years; (Hjartardóttir et al., 2016)), while the assumed depths derive from seismic evidence for a basaltic magma chamber or a system of interconnected dikes and sills between 3 and 7 km depth (Einarsson, 1978; Einarsson and Brandsdóttir, 1980; Kennedy et al., 2018). The sills and crust in this simulation were both composed of dry (0.1 wt% H_2O) basalt. The effects of hydrating the crust are explored with the Magma Chamber Simulator (MCS).

Once the capacity and location of partial melt production was constrained by the thermal model, MCS models were used to investigate the consequences of the resulting thermal conditions on the compositions of wallrock partial melts produced in the vicinity of basaltic intrusions. The MCS uses algorithms constrained by experimental thermodynamic datasets to predict magma chamber chemical evolution during fractional crystallization plus crustal assimilation and/or magmatic recharge (Bohrson et al., 2014; Bohrson and Spera, 2001). Mývatn Fires basalt ($\delta^{18}O = \sim + 5.0$‰; this work) was used as the starting magma composition. Models were run for simultaneous fractional crystallization and assimilation of partial melt using a range of wallrock compositions. In cases where rhyolitic magmas were produced, the resulting compositions were used in a simple isotopic mixing model to estimate the resulting $\delta^{18}O$ of the final magmas given different average $\delta^{18}O$ values of the assimilated crust (0‰, −5‰, and − 10‰). The goal of this combined modeling technique was to find the parameters and conditions that allow for production of magmas that most closely match the Krafla rhyolites, and to quantify the roles of fractional crystallization, partial melt production and assimilation in the system.

3. Results

3.1. Zircon U-Th and $\delta^{18}O$ analyses

SHRIMP-RG ^{238}U-^{230}Th-^{232}Th dating of individual zircon grains in three post-caldera rhyolite domes yielded crystallization ages of 88.7 ± 9.9 ka for Jörundur, 83.3 ± 9.2 ka for Hlíðarfjall, and 85.5 ± 9.4 ka for Gæsafjallarani (Fig. 6). Each dome has a unimodal age distribution. The ages of the domes overlap within error. Our ages overlap with the $^{40}Ar/^{39}Ar$ eruption ages between 83 and 90 ka from Sæmundsson and Pringle (2000), but are younger than the prior U-Th dating from Gæsafjallarani which yielded an age estimate of ~120 ka. (Carley et al., 2020).

Individual zircon grains yielded overlapping and low $\delta^{18}O$ values between +0.5 to +2.0‰ (Fig. 7) for all three domes. For all zircons analyzed, intragrain variability is less than the analytical uncertainty (± 0.25‰, 2σ), but population heterogeneity (1.8‰) overall exceeds the expected analytical uncertainty (± 0.5‰, 2σ) (Fig. 6). Zircons extracted from Jörundur range from +0.69 to +1.71‰ with an average of +1.24‰, Hlíðarfjall zircons range from +1.07 to +1.79‰ with an average value of +1.45‰, and Gæsafjallarani zircons exhibit the largest range from +0.59 to +1.98‰ with an average of +1.27‰ (Fig. 7).

Under cathodoluminescence imaging (CL; Fig. 5, Supplement Fig. A), two distinct morphological types are identified in the zircon populations. Each dome has a population of equant grains and a second population of elongated grains. A subpopulation of equant grains exhibit sector zoning (Fig. 5). These morphologies do not vary systematically in $\delta^{18}O$. Overall, we observe no trend in $\delta^{18}O$ vs U-Th age within any of the zircon populations (Supplement, Fig. A), other than consistently low $\delta^{18}O$ values across the crystallization event (Fig. 7). We observe no systematic variations between inner parts of zircon grains and outer portions of the same grain.

3.2. Trace elements in zircons

Zircon U, Th, Hf, and Yb concentrations exhibit strong correlation to the behavior predicted during fractional crystallization given known partition coefficients for zircon; Hf/Yb shows a sharp initial decrease and overall downward trend as Th/U increases (Fig. 8A), consistent with the extreme compatibility of Hf and greater compatibility of U relative to Th in zircon. To assess whether fractional crystallization is indeed responsible for this trend, we undertake trace element modeling of magma differentiation as recorded by zircon, using the following

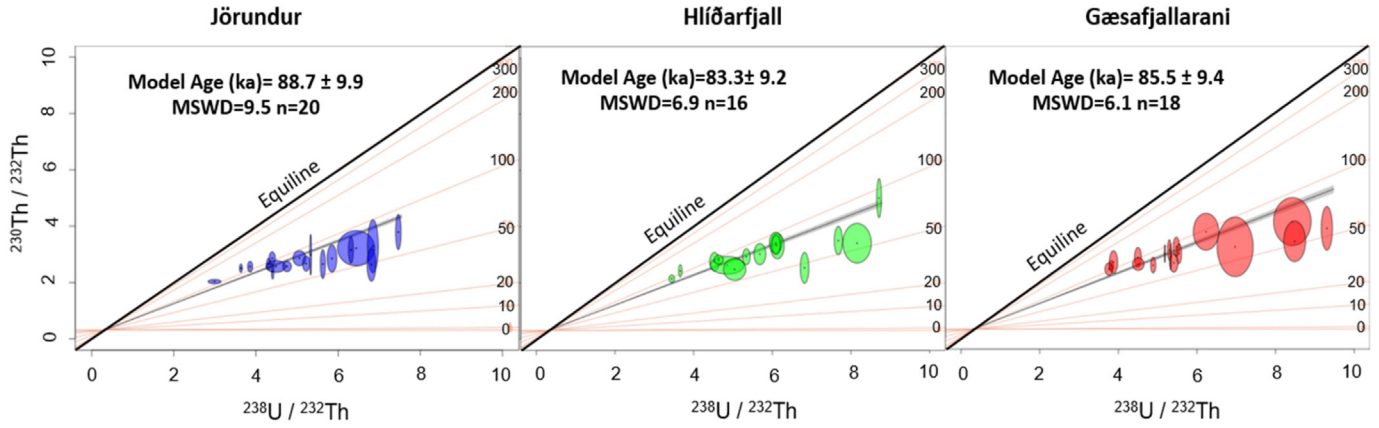

Fig. 6. Zircon Isochron. Zircon isochron diagram showing the U-Th model ages of the zircon populations in the three domes. Error ellipses show 2σ error. Best fit lines show the estimated isochron model age for each dome. Jörundur $^{238}U/^{232}Th = 0.3068 \pm 0.01$, Hlíðarfjall $^{238}U/^{232}Th = 0.3059 \pm 0.01$, Gæsafjallarani $^{238}U/^{232}Th = 0.3051 \pm 0.01$. n = Number of zircons analyzed. MSWD = Mean square weighted deviation. Red isochron labels are reported in thousands of years (ka). (For interpretation of the references to colour in this figure legend, the reader is referred to the web version of this article.)

partition coefficients: $Kd_{Hf} = 1200$, $Kd_{Yb} = 11$, $Kd_U = 46$, $Kd_{Th} = 14$. These values were estimated from experimental data (~850–900 °C; Melnik and Bindeman, 2018) and from values reported in the GERM partition coefficient database for zircons in high silica rhyolites (GERM, 2015). The Yb partition coefficient value also considers the partitioning of Yb into other phases, such as apatite (an accessory phase in all Krafla rhyolites; Rooyakkers, 2020). We assume that the other elements considered here predominantly partition into zircon (Clayborne et al. 2018; Melnik and Bindeman, 2018). These calculations specifically model how much zircon crystallization is needed to form the observed trace element trend in zircon grains; this is therefore a minimum estimate for the total amount of fractional crystallization that these rhyolites may have undergone since zircon saturation.

Most of our data are consistent with ~1–2% zircon fractionation. Some grains have compositions consistent with up to 6% fractional crystallization, and rare grains with 10–20% crystallization (Fig. 8B and C). However, changes in the partition coefficient values can significantly affect the estimated amount of crystallization predicted by the model; for example, lowering the partition coefficients for Yb and Th by an order of magnitude results in an estimate of around 10–15% of fractional crystallization. Regardless of the Kd values selected, the overall trend predicted by the FC model provides an excellent fit to the observed trace element trends, supporting a central role for FC in magmatic differentiation after zircon saturation.

3.3. Zircon crystal size distributions (CSD)

Zircon CSDs are concave-down (Fig. 9), with maxima around 10–200 μm. We analyze the right-hand sides of the curves (the portions with negative slopes), as they reflect the conditions of zircon crystallization, while the left-hand sides (positive slopes) show trends previously attributed to crystal coarsening via temperature cycling (Simakin and Bindeman, 2008). CSDs for the three dome samples are comparable but not overlapping (Fig. 9). The sample size for KRF10 (Jörundur) is too small ($n = 42$) for statistical significance of the largest size bins but shows a steep slope and small mode relative to the distributions

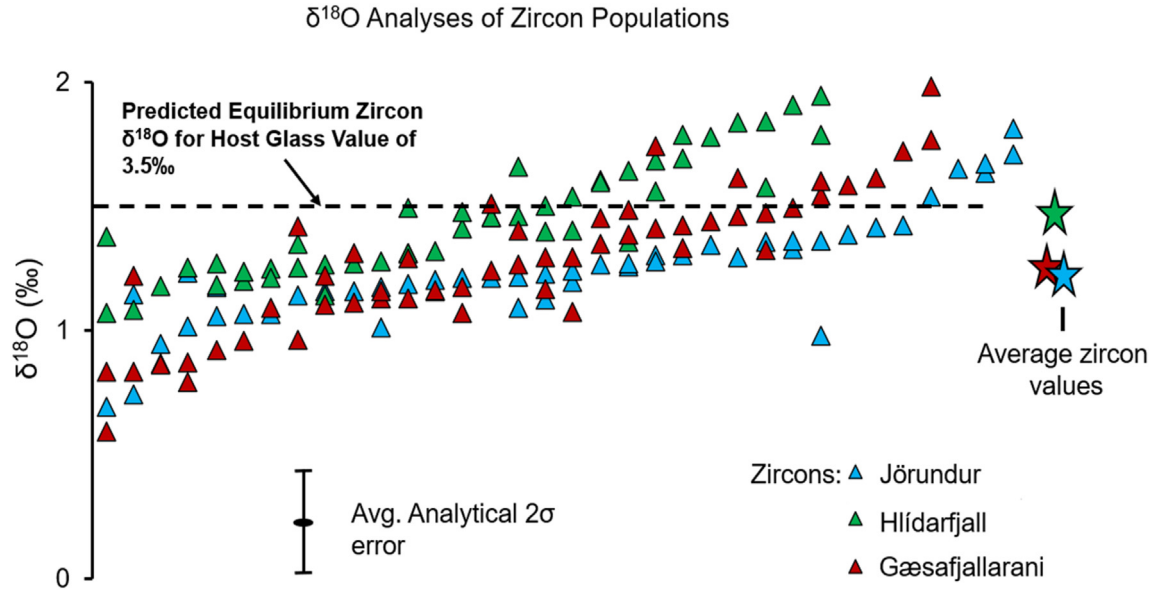

Fig. 7. $\delta^{18}O$ of Dome Zircons. $\delta^{18}O$ (‰) presented for the three rhyolite domes zircon populations (for each dome, each vertical array consists of multiple spot analyses from an individual grain). The expected equilibrium zircon $\delta^{18}O$ based on a host melt value of +3.5‰ and $\Delta^{18}O$(melt-zircon) = 2‰, is shown (assuming a magmatic temperature of 900 °C; e.g. Bindeman, 2008), as well as average values for the respective zircon populations.

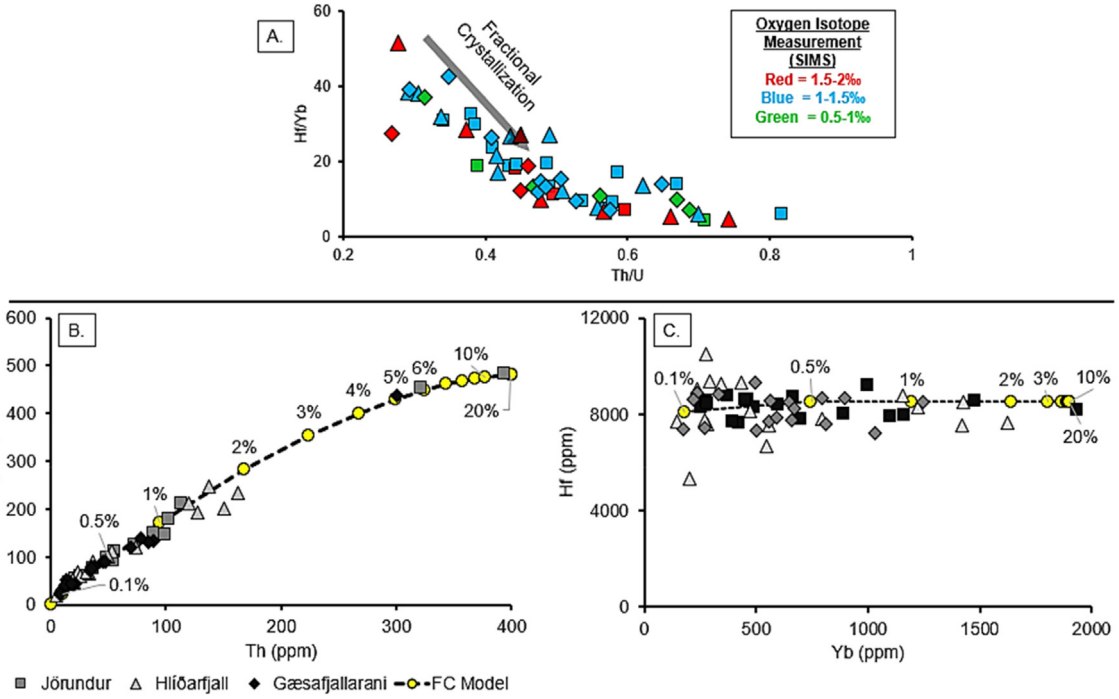

Fig. 8. Zircon Trace Elements. A) Hf/Yb versus Th/U trace element ratios measured by SHRIMP-RG on individual zircon grains. Shapes represent the dome the zircon was extracted from (see legend at bottom of figure). Colors indicate the measured $\delta^{18}O$ (Red = +1.5 to +2‰, Blue = +1 to +1.5‰, and Green = +0.5 to +1‰). B) Zircon Th vs. U concentrations (no oxygen isotope information shown on B and C). C) Zircon Yb vs. Hf concentrations. B) and C) are accompanied by a fractional crystallization (FC) model using the equation $Cl/Co = (1\text{-}F)^{(D-1)}$, where F is the fraction of material crystallized and D is the bulk partition coefficient for each element. Partition coefficients for FC are from Melnik and Bindeman (2018), assuming temperatures of ~850–900 °C: $Kd_{Hf} = 1200$, $Kd_{Yb} = 11$, $Kd_{U} = 46$, $Kd_{Th} = 14$. Percentages indicate the amount of crystallization that has occurred at each composition. (For interpretation of the references to colour in this figure legend, the reader is referred to the web version of this article.)

from the other domes (Fig. 9). The populations imaged for Hlíðarfjall and Gæsafjallarani have *n* large enough to be statistically significant. The distribution for Hlíðarfjall is skewed further to larger values than either of the other domes and shows a shallower slope, indicative of a longer crystallization time, assuming similar growth rates for each dome (Fig. 9). Gæsafjallarani has a distribution that trends towards smaller values and a steeper slope (Fig. 9).

To attain the most accurate estimates for residence times from our CSD data, zircon growth was modeled using the code of Bindeman and Melnik (2016), which parameterizes zircon growth as a function of cooling rate for intrusions of various sizes. Based on input temperatures and the observed zircon sizes, the model suggests that zircons mostly grew at a rate of $G = 10^{-14}$ cm/s, given the size of the inferred cooling magma bodies (Bindeman and Melnik, 2016; Melnik and Bindeman, 2018). Using this growth rate, we estimate the residence times of these zircons in their host melt using the relationship:

$$\text{CSD Slope} = -\frac{1}{\text{Growth Rate}\left(\frac{cm}{s}\right) * \text{Residence Time } (s)}$$ (Cashman and Marsh, 1988; Marsh, 1988).

Measured slopes on the right-hand side of the CSDs are between −125 and − 143 μm^{-1} (Fig. 9), yielding crystallization time estimates of 2500 yrs. and 2200 yrs. for Hlíðarfjall and Gæsafjallarani, respectively. If growth rates are increased an order of magnitude to 10^{-13} cm/s, (rapid growth possibly suggested by the presence of elongated crystals), corresponding with exceptionally fast cooling in thin magma sheets, these times are reduced to ~250 and ~ 200 yrs.

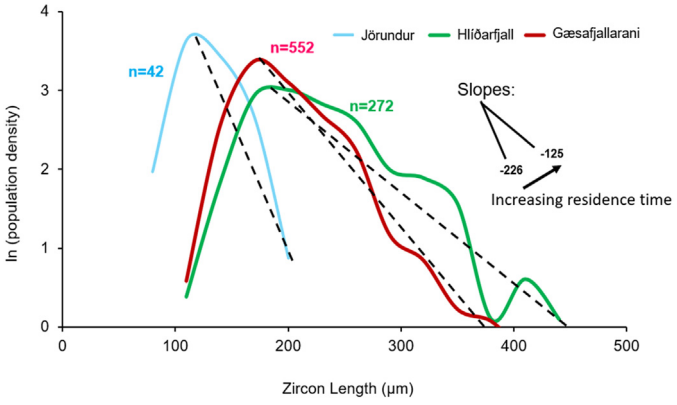

Fig. 9. Zircon Crystal Size Distribution. Natural logarithm of the population density for zircons of different lengths (longest axis, in μm) from each dome. There is a linear trend between elongation and size (not shown here), implying that there is no bias towards sampling large zircons. The gradients (population density/μm) of the downward-sloping parts of the curves are used to estimate residence times.

3.4. Oxygen isotope measurements of pyroxene, plagioclase, and groundmass

Laser fluorination $\delta^{18}O$ analyses for Jörundur yielded values of +3.55‰ for groundmass, +2.67‰ and + 1.99‰ for plagioclase, and + 1.12‰, +1.59‰, and + 2.22‰ for pyroxene (Fig. 10; Table 1). Plagioclase that is in $\Delta^{18}O$ (melt-plag) isotopic equilibrium would be expected to have a $\delta^{18}O$ of +2.5‰ (Bindeman, 2008) (Fig. 7) within error of one +2.67‰ crystal value, while another crystal of plagioclase with $\delta^{18}O$ = +1.99‰ is below that expected at equilibrium (Fig. 10; Table 1). By contrast, only one bulk analysis of pyroxenes has a $\delta^{18}O$ value around the predicted equilibrium value of +1.5‰ (Fig. 10; Table 1).

Hlíðarfjall has a groundmass $\delta^{18}O$ of +3.44‰ (Fig. 10; Table 1), within error of the groundmass value for Jörundur, and thus equilibrium $\delta^{18}O_{Plag}$ and $\delta^{18}O_{Px}$ are expected to be +2.5–2.7‰ and + 1.5–1.7‰ respectively at ~900 °C. However, a single bulk pyroxene analysis had a $\delta^{18}O$ value of +4.75‰, significantly above the equilibrium value.

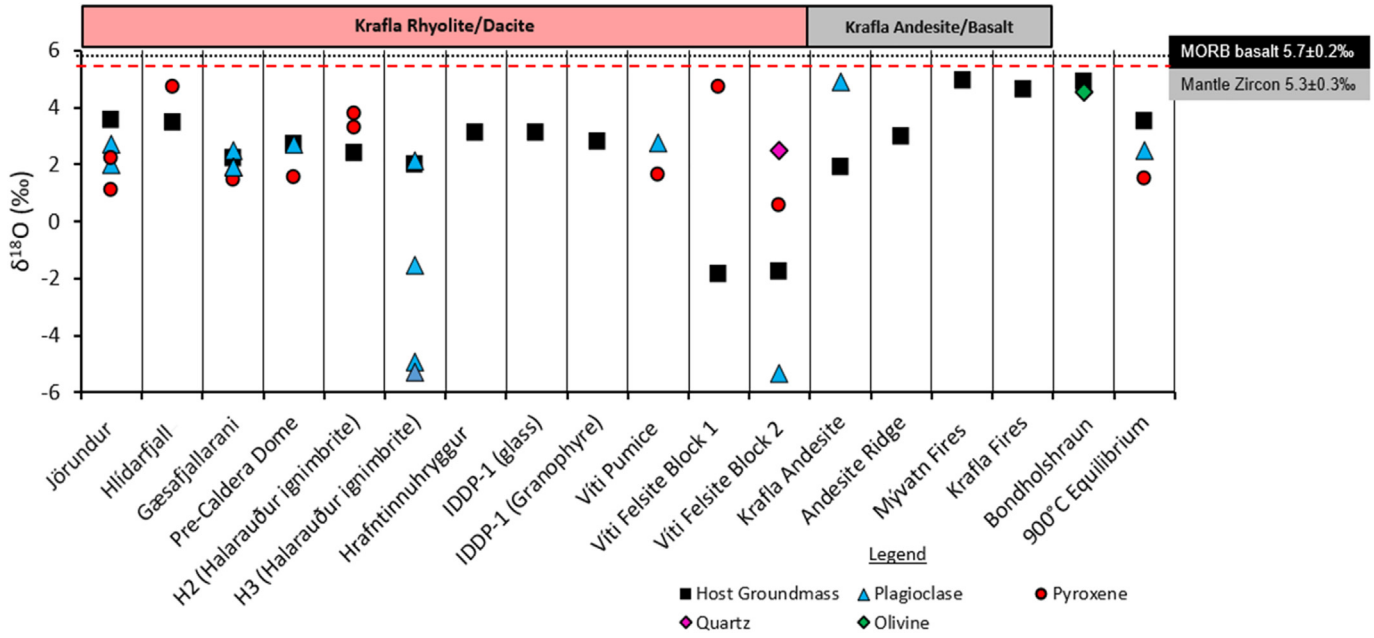

Fig. 10. $\delta^{18}O$ of All Units and All Phases. $\delta^{18}O$ of groundmass, plagioclase, pyroxene (measured by laser fluorination) in all analyzed units at Krafla. Average MORB basalt and mantle zircon values are from Valley et al. (1994).

The sample of Gæsafjallarani groundmass exhibits notably more perlitic and hydrated textures than the samples from the other two domes. The resulting $\delta^{18}O$ is lower than the other two domes at +2.21‰, but we infer that this difference most likely reflects *syn*- or post-emplacement alteration processes rather than a true magmatic difference in isotopic composition (Fig. 10). Three measurements of single plagioclase crystals gave slightly diverse $\delta^{18}O$ values of +2.49‰, +1.92‰ and + 1.91‰, and a bulk analysis of several pyroxene grains returned a value of +1.48‰ (Fig. 10; Table 1).

The pre-ignimbrite dome (sample KRF-1.2) gave a groundmass $\delta^{18}O$ value of +2.68‰, but also exhibits hydrated perlitic textures indicative of syn- or post-emplacement processes that may have altered the original magmatic value to slightly lower $\delta^{18}O$. Plagioclase extracted from this sample returned a $\delta^{18}O$ of +2.70‰, and two pyroxene analyses gave values of +1.56‰, and + 1.66‰ (Fig. 10; Table 1).

Groundmass $\delta^{18}O$ values for the Halarauður ignimbrite are +2.38‰ in the intermediate unit H2 of Rooyakkers et al. (2020), and + 1.96‰ in the basaltic zone (unit H3). In H2, pyroxenes clustered in a population at +3.31‰, +3.52‰, and + 3.78‰ (Fig. 10), requiring a + 4.5 to +5‰ equilibrium melt value, thus out of equilibrium with H2 melt. In H3, 5 individual plagioclase measurements returned a wide range of values from −5.26‰ to +2.13‰ (equilibrium ~ + 1‰) (Fig. 10).

The phase 3 Hrafntinnuhryggur and IDDP-1 rhyolites both gave host glass $\delta^{18}O$ values of +3.10‰. The granophyre from the IDDP-1 well had a bulk value of +2.80‰ (Fig. 10). Plagioclase and pyroxene in pumice from Víti crater gave $\delta^{18}O$ values of +2.72‰ and + 1.62‰, respectively (Fig. 10). Glass $\delta^{18}O$ values in felsite xenoliths also erupted from Víti were low, at −1.84‰ and − 1.08‰ (Fig. 10). Other phenocrysts from the felsite spanned a large range, from an extremely low −5.35‰ value to near mantle values of +4.75‰ (Fig. 10).

3.5. Thermal modeling results

Fig. 11 shows the time-temperature paths for different depths in the Heat2D thermal model. Near the sill intrusions between 4 and 6 km depth, temperatures are elevated above the dry basaltic solidus (~1100 °C), allowing for small degrees of partial melting (Fig. 11C). In these zones along the boundary of the magma chamber, the thermal model predicts melt fractions between 0.2 and 0.4 (Fig. 11D). The $\delta^{18}O$ of this partial melt would reflect the crust that it was partially melted from and would therefore have low $\delta^{18}O$ values between 0 and − 12‰.

Away from the main area of heat and sill intrusions, temperatures decrease but the overall geothermal gradient remains elevated. Crust 1000 m above the intrusion (3 km depth) is heated to a maximum temperature of 700 °C, while crust further away (1–3 km above the intrusion) is barely impacted by the heat of the intrusion (Fig. 11).

3.6. Magma chamber simulator results

The first experiment tested by the MCS is the simple case of basaltic magma at $T = 1200$ °C intruding into dry basaltic crust at ~10 km depth (3000 bars) (Fig. 12). In this case, minimal partial melting occurs, with the model estimating less than 1% (by total mass of the magma chamber) assimilation of partial melt (Fig. 12). Without generation and assimilation of any high silica partial melt and remaining at a depth where the magma is too hot to crystallize substantially, the magma undergoes minimal differentiation or change in oxygen isotope composition. The result is a near normal $\delta^{18}O$ basaltic magma (Fig. 12).

The next scenario is crust with 1 wt% H_2O (composition from Spulber and Rutherford, 1982). In simulations using this composition at both 2000 and 3000 bars, around 10% (by mass of the total magma chamber) partial melt is produced and assimilated (Fig. 12). The partial melt composition predominantly dacitic (Fig. 13). Coupled with subsequent FC, the intruding basaltic magma undergoing assimilation can differentiate to a small volume (20% of original magma chamber mass remains as melt) of dacite (Fig. 13). Depending on the average $\delta^{18}O$ value of the crust that is partially melted, this resulting dacite can have a $\delta^{18}O$ as low as +3.7‰ (assimilant of −10‰) to as high as +5.0‰ (assimilant of 0‰) (Fig. 13B).

Although the crust at Krafla is predominantly basaltic, drilling has revealed occasional intermediate to silicic intrusive and extrusive rocks at depth (Hattori and Muehlenbachs, 1982; Pope et al., 2013; Weisenberger et al., 2015). Hence, to test the effect of a more evolved assimilant, we modeled assimilation of a dry andesitic wallrock composition at 3000 bars and compared it to the dry basalt case (Fig. 12). The more evolved composition results in more partial melting (up to 17% by

Table 1
Results of Laser Fluorination $\delta^{18}O$ Analyses. *indicates a single crystal analysis, all other analyses are multiple crystals. Predicted equilibrium $\delta^{18}O$ at 900 °C is shown for a host glass value of 3.5‰ (Bindeman, 2008).

Sample	KRF-10	KRF-20	KRF-21	KRF-1.2	KRF-1	KRF-2	KRF-14	IDDP-1 (glass)	IDDP-1 (Granophyre)	IC-81	IC-82	IC-83	KRF-13	KRF-5	IC-78	IC-79
Unit	*Jörundur*	*Hlíðarfjall*	*Gæsafjallarani*	*Pre-Caldera Dome*	*Halarauður ignimbrite*	*Halarauður ignimbrite*	*Hrafntinnuhryggur*	*Drill Core Intercepted Rhyolite*	*Granophyre (drillcore)*	*Viti Pumice*	*Viti Felsite Block 1*	*Viti Felsite Block 2*	*Krafla Andesite*	*Andesite Ridge*	*Mývatn Fires*	*Krafla Fires*
Rock Type	Rhyolite	Rhyolite	Rhyolite	Rhyolite	Dacite/Intermediate	Basalt	Rhyolite	Rhyolite	Granophyre	Rhyolite	Rhyolite	Rhyolite	Andesite	Andesite	Basalt	Basalt
Glass (‰)	3.55*	3.44*	2.21*	2.68*	2.38*	1.96*	3.28*	3.1*	2.59*		−1.84*	−1.76*	1.9*	3*	4.92*	4.62*
							2.92*	3.1*	2.97*			1.13*				
												−2.61*				
Plagioclase	2.67*		2.49*	2.7		−4.93*				2.72		−5.35	4.9			
(‰)	1.99*		1.92*			2.13*										
			1.91*			−1.57*										
						−5.26*										
						−5.06*										
Pyroxene	1.12	4.75	1.48	1.56	3.78					1.62	4.75	0.54				
(‰)	1.59			1.66	3.52											
	2.22				3.31											
Olivine (‰)												2.46				
Quartz (‰)																
						Glass			Plagioclase							Pyroxene
Equilibrium (900 °C)						3.5			2.5							1.5

mass of the magma chamber). The final magma composition after the completed AFC process is a basaltic andesite (54% SiO_2) with a $\delta^{18}O$ of +2.8‰ to +4.5‰, depending on the chosen value for the assimilant (Figs. 12 and 13).

The final scenario modeled was intrusion of basaltic magma into basaltic crust that has experienced extensive hydrothermal alteration. This scenario was modeled at several pressures, starting with a shallow simulation at 1000 bars where the average value of altered oceanic crust (newly formed MORB that has interacted with seawater) was used as the wallrock composition (Kuo, 2017). At higher pressures, between 2000 and 4000 bars, we used an amphibolite wallrock composition with 5 wt% H_2O (composition from Wolf and Wyllie, 1995). Between 15% and 43% (by mass) partial melt is created and assimilated in these scenarios. With additional fractional crystallization, this scenario produces a final magma of dacitic composition (Fig. 12). An assimilant with $\delta^{18}O$ of −10‰ produces final magmatic $\delta^{18}O$ values that are lower than those observed for the Krafla rhyolite domes when partial melting is increased (Fig. 13B). In the case with the largest amounts of partial melt formation (amphibolite wallrock at 4000 bars, 45% by mass partial melting and assimilation; Fig. 12), the final $\delta^{18}O$ of the resulting magma is lower than values observed for the domes, regardless of assumed average crustal $\delta^{18}O$ (Fig. 13). When a wallrock $\delta^{18}O$ of −5‰ is assumed, the final magmatic $\delta^{18}O$ produced by the AFC process at 1000 to 2000 bars (hydrated basalt, AOC, or amphibolite wallrock compositions) provides a good fit for the measured $\delta^{18}O$ value of the domes (Fig. 13B). Wallrock with a $\delta^{18}O$ of 0‰ also provides a good fit in the 3000 bars amphibolite wallrock model (Fig. 13B).

In all models, the initial partial melts are dacitic to rhyolitic, but further partial melting at higher temperature produces less evolved dacitic to intermediate compositions (Fig. 12A). Importantly, none of the modeled partial melt compositions overlap with the observed chemistry of the Krafla rhyolites (Fig. 12A and C). Furthermore, none of our AFC simulations produced a high-silica, low $\delta^{18}O$ rhyolite as the final product during isobaric differentiation (Fig. 12). Instead, the final magmas after AFC has allowed the wallrock to thermally equilibrate with the magma are mainly low $\delta^{18}O$ andesites-dacites.

4. Discussion

4.1. Magmatic evolution of the rhyolite domes

The ca. 80 ka rhyolite domes studied here were erupted ca. 20–30 ka after the Halarauður caldera collapse event. Whole-rock compositions of Halarauður products transition up-section from mildly basalt-contaminated rhyolite to hybrid intermediate compositions and finally to homogeneous basalt, implying that the rhyolite tapped in this event was completely evacuated (Rooyakkers et al., 2020). We thus infer that the domes represent a renewed episode of rhyolite production after caldera collapse rather than residual rhyolitic magma left over after the Halarauður eruption.

Our zircon analyses reveal close similarities among the three rhyolite domes. Trace element compositions for zircons from all three domes overlap and show similar trends that are consistent with modeling of zircon fractional crystallization (Fig. 8), while zircon $\delta^{18}O$ values have similar averages and ranges across the three domes (Fig. 7); values measured for Hlíðarfjall (average $\delta^{18}O$ = +1.45‰, range = 1.06–1.94‰) are well within 2σ error (± 0.25‰) of those measured in Jörundur and Gæsafjallarani (Fig. 7), although the higher average may suggest a slight difference from the other domes (Fig. 7). Similarly, overlapping zircon U-Th zircon crystallization ages for all three domes imply a close link between them. Based on these chemical and temporal overlaps, we suggest that the zircon populations from all three domes likely crystallized during the same cooling event. This scenario is consistent with other similarities in their whole-rock and mineral compositions, which imply that the three domes ultimately derive from a common magma body as defined by compositional trends

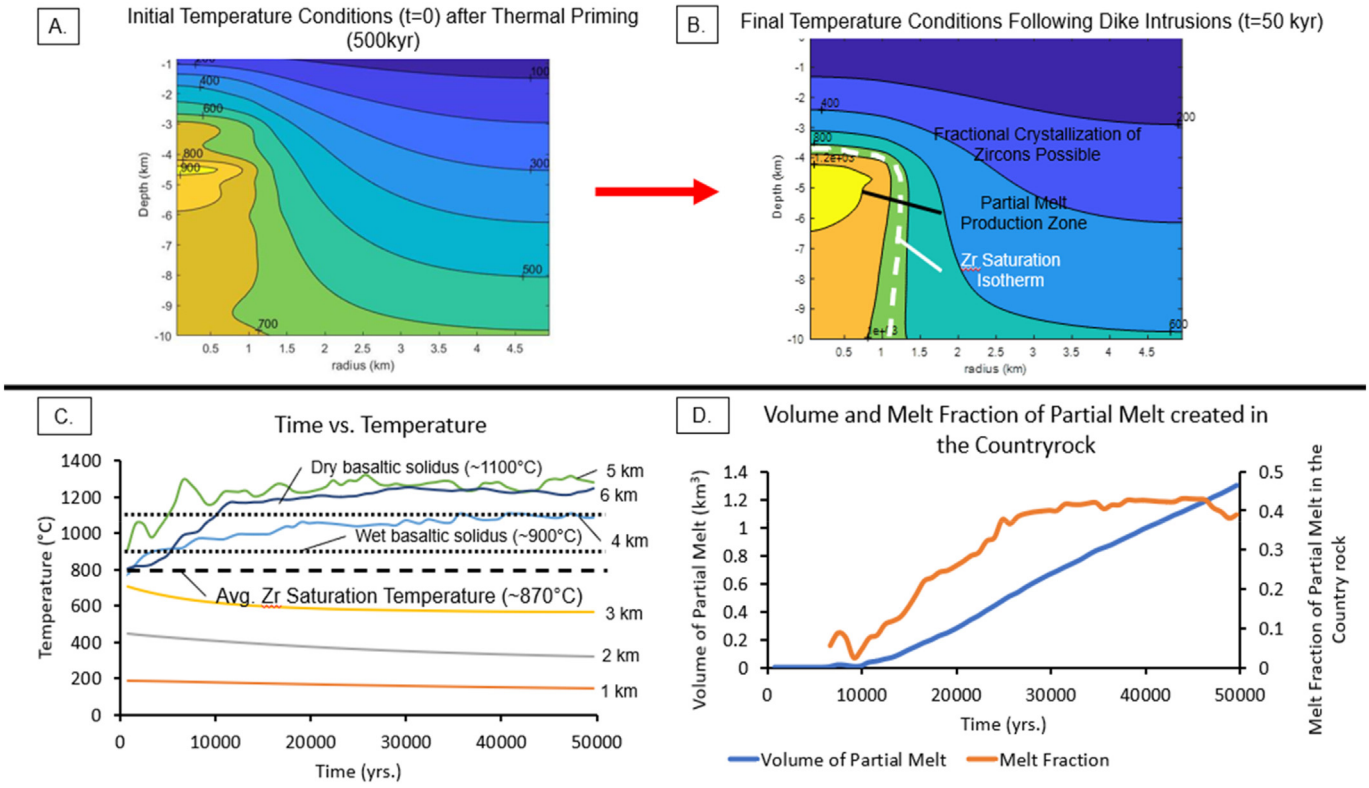

Fig. 11. Thermal Model Time-Temperature Paths and Partial Melt Volumes. A) Temperature profile of the crust at time $t = 0$,after 500 kyr of thermal priming has created an elevated geotherm. B) The final temperature profile after 50 kyr of intrusions. C) Time-temperature paths at different depths within the thermal model run at the radius just outside of the intrusion (x = 0.5 km). The zircon saturation temperature and the wet/dry basaltic solidus are also shown. D) Maximum melt fraction reached in the domain of the crust modeled and the volume of partial melt created in the crust calculated using cylindrical coordinates and assuming radial symmetry of the 2D space. Location of partial melt generated in the system can be evaluated by melt contours that store the volume of melt for each cell and each time step in the model. Near the magma chamber, melt fraction will increase while further away from the chamber melt fraction will decrease. Zircon saturation temperatures are calculated based on the whole rock compositions of the rhyolite domes according to the model of Boehnke et al. (2013).

(Rooyakkers, 2020). A slight difference in average zircon age between Hlíðarfjall and the other domes may indicate slightly longer crustal residence for Hlíðarfjall, consistent with our CSD data and its slightly more evolved whole-rock and phenocryst compositions (Rooyakkers, 2020). Overall, we conclude that the three domes are likely related to the same original low $\delta^{18}O$ magma batch, but the late-stage evolution of the Hlíðarfjall magma appears to have taken a slightly different differentiation path to the other two domes.

The average $\delta^{18}O$ values of the zircon populations from the domes suggest crystallization from a host melt $\delta^{18}O$ value of ~ + 3.0 ± 0.5‰, assuming isotopic equilibrium; the measured values of the glass in the three domes is consistent with this equilibrium value. These +0.5–1.5‰ zircon $\delta^{18}O$ values are very low by global standards, 4–4.5‰ lighter than normal mantle values of +5.3 ± 0.3‰ (Valley et al., 1994), and require either crystallization from low $\delta^{18}O$ host melts, or assimilation directly from hydrothermally altered wallrock. Although each zircon population shows minor variability in $\delta^{18}O$, greater than the analytical uncertainty (±0.2‰. 1 st. dev.), the $\delta^{18}O$ values do not vary systematically along the inferred fractional crystallization trend (Fig. 8). This suggests that zircons grew from an already low $\delta^{18}O$ magma that was not systematically changing in $\delta^{18}O$ during crystallization, and therefore not incorporating new low $\delta^{18}O$ material, at the time of zircon growth. We thus infer that zircon growth occurred during the later stages of rhyolite differentiation, after significant assimilation of altered low $\delta^{18}O$ crust had ceased. We attribute the slight heterogeneity in zircon $\delta^{18}O$ to minor isotopic heterogeneity within a poorly mixed magma body; ~1–1.5‰ variation in melt $\delta^{18}O$ is required to explain the zircon variability. Overall, the zircon populations of the Krafla rhyolite domes are more isotopically homogeneous than populations analyzed from other Icelandic rhyolites (e.g. Askja, Torfajökull, Hekla; Bindeman et al., 2012), but show comparably low $\delta^{18}O$ values (Carley et al., 2020; Carley et al., 2014; Reimink et al., 2014).

Based on predicted equilibrium values (Fig. 10), it appears that some pyroxene and plagioclase grains in the dome rhyolites, like the zircons, crystallized in equilibrium with their host melts. Occasional instances of marked disequilibrium, such as a bulk analysis of pyroxenes from Hlíðarfjall that gave a close to mantle-like $\delta^{18}O$ value, or plagioclase with strongly negative $\delta^{18}O$ values, provide evidence for assimilation of normal $\delta^{18}O$ cargo and hydrothermally altered rocks with low $\delta^{18}O$ cargo (Fig. 10; Table 1). Together, these observations suggest that more than one process is acting to differentiate these magmas.

4.2. Modeling perspectives on petrogenesis of the rhyolite domes

Our combination of thermal and chemical modeling suggests that segregation of partial melt from around the margins of basaltic magma bodies (sensu Jónasson, 1994; Fig. 4A) is not a viable mechanism to generate the rhyolitic dome magmas. We recognize two challenges to this process. Because most of the volume of partial melt in the thermal model was created within only 1–10 m of the boundary of the basaltic intrusion (Fig. 11), the first difficulty is in producing sufficient volumes of high silica partial melt partial melt. While our MCS models show that hydrothermal alteration can encourage more partial melting in the crust, the estimates calculated from the thermal model provide a minimum estimate for the volume of partial melt created in the crust surrounding a magma body and therefore represent the most evolved composition of partial melt that can be generated. Greater degrees of partial melting in altered or hydrated crust results in

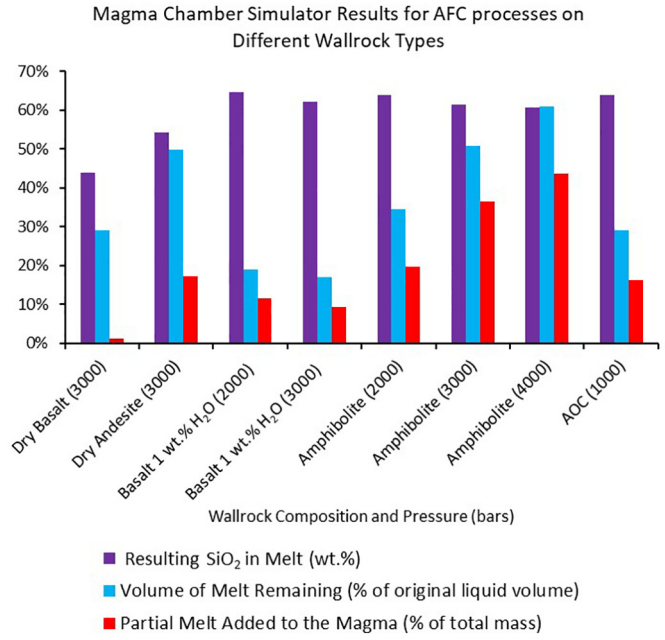

Fig. 12. Magma Chamber Simulator (MCS) Results. Results of assimilation and fractional crystallization (AFC) runs on the magma chamber simulator, showing SiO_2 content of the final magma, the magma volume remaining after AFC (% of original liquid volume), and the amount of partial melt added to the magma (% of total mass). For each run, basaltic magma (Mývatn Fires composition of Thorarinsson, 1979) with T = 1200 °C is intruded into wallrock of specified composition (detailed on x-axis, with model pressures in bars given in parentheses). Calculations for dry (0.1 wt% H_2O) basaltic magma were run at and 3000 bars using wallrock of identical composition. The dry andesite (0.1 wt% H_2O) wallrock composition is equivalent to the erupted andesite unit that we sampled inside the southern caldera margin. The basaltic wallrock composition with 1 wt% H_2O was taken from Spulber and Rutherford's (1982) experiments on partial melting of Icelandic crust. The amphibolite composition is from Wolf and Wyllie (1995) and has 5 wt% H_2O.

less-evolved partial melt compositions, which is thus even less likely to produce the observed composition of the Krafla rhyolites. Therefore, to assess whether sufficient volumes of high silica partial melt with a composition similar to that of the Krafla rhyolites can be produced purely by partial melting, we evaluate the partial melt volumes produced in the dry crust of the thermal model.

The collective erupted volume of the three domes is ~0.7 km^3 (Jónasson, 1994). Assuming that this erupted volume represents only a fraction of the total magma body volume, for example around ~1/3 of the magma produced below the surface, we suggest that a total volume of >2 km^3 of rhyolite would be required to feed eruption of the domes. Over the full 50 kyr thermal model run, ~1.3 km^3 of high silica partial melt is produced; over the 20–30 kyr between the Halarauður and dome eruptions this reduces to 0.8 km^3 (Fig. 11). Unless almost the entire volume of partial melt was segregated over this 20–30 kyr period and completely drained on eruption, our models suggest insufficient partial melting occurs to produce the dome eruptions.

The second challenge is in producing the compositions of the dome magmas purely by partial melting. The MCS predicts that the partial melt itself, while low in $\delta^{18}O$, is mostly dacitic in composition and does not overlap with the rhyolitic composition of surface lavas (Fig. 13A). The closest match to the measured whole rock compositions comes from the initial (very low melt fraction and small volume) partial melting of the average altered oceanic crust composition or the andesitic wallrock composition, but even these partial melt compositions do not overlap with the rhyolite compositions of the domes or other Krafla rhyolites in any major element dimension (Fig. 13A and C). If silicic partial melt were segregated from these zones, further differentiation would then be required to reach the observed rhyolitic compositions. Furthermore, at high temperatures, the $\delta^{18}O$ of the protolith will be roughly equal to the $\delta^{18}O$ of any partial melt produced (Hoefs, 2015), so partial melting of the Krafla crust will produce a melt that takes on the low values of the crustal material, between 0 and − 12‰ for altered rocks at Krafla (Hattori and Muehlenbachs, 1982). These values are far

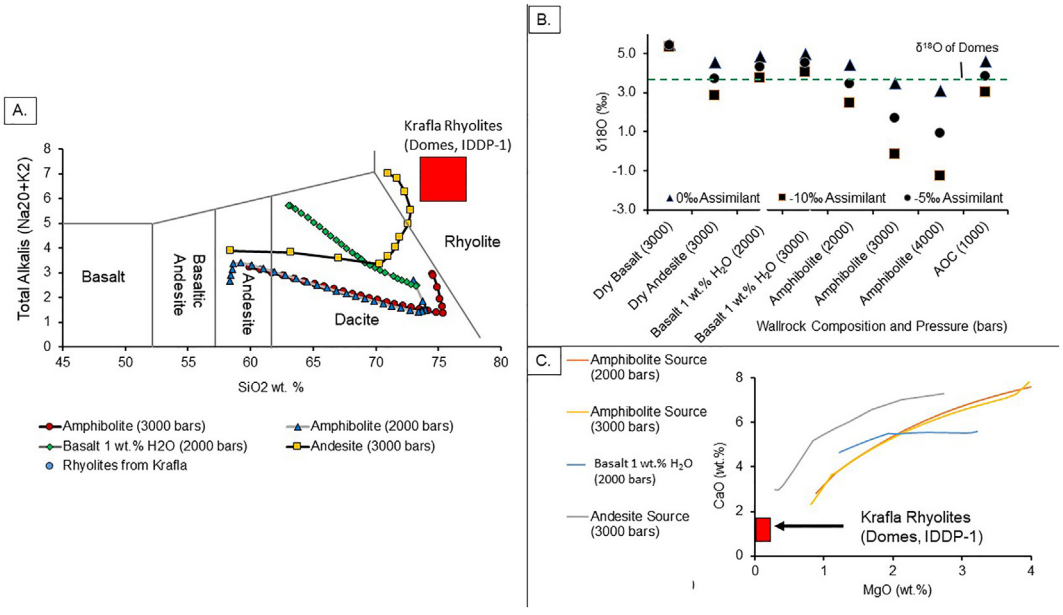

Fig. 13. Magma Chamber Simulator Analysis. A) Wallrock partial melt compositions produced in selected MCS simulations for different wallrock compositions and pressures. Symbols indicate 5 °C temperature cooling increments and the partial melt compositions produced by melting of the protolith indicated in the legend. Initial partial melts have the most evolved compositions, moving towards less evolved compositions at higher degrees of melting. None of the simulated partial melt compositions overlap with the observed compositions of the rhyolites, and most of the partial melt is dacitic rather than rhyolitic. B) Final magmatic $\delta^{18}O$ values after AFC, calculated from MCS results with an isotopic mixing model assuming different average $\delta^{18}O$ values for the crustal assimilant (−10‰, −5‰ and 0‰). Pressures of MCS simulations in bars are given in parentheses. C) The compositions of the partial melt created during MCS simulations in each scenario. None of the partial melt compositions overlap with observed compositions of the Krafla rhyolites (red square). (For interpretation of the references to colour in this figure legend, the reader is referred to the web version of this article.)

lower than the measured $\delta^{18}O$ of any of the domes or any other Krafla rhyolites, which have groundmass values between +3 to +3.5‰ (Table 1).

The isotopic compositions of the domes are more consistent with an AFC scenario. For example, producing the observed rhyolitic groundmass $\delta^{18}O$ value of ~ + 3 to +3.5‰ by assimilating partial melt with a low $\delta^{18}O$ of −5.0‰ into a normal $\delta^{18}O$ magma of +5.0‰ requires 40% assimilation by total mass of the magma chamber. If the magma chamber, therefore, has a total volume of at least 2 km^3, then the necessary 40% by mass assimilation corresponds with a volume of ≥0.8 km^3 of partial melt. This volume of partial melt is well within the amount predicted by the thermal model in the time constrained by the geochronology (Jónasson, 1994; Zierenberg et al., 2013) (Fig. 11B). If more assimilation occurs, the resulting $\delta^{18}O$ value may be too low, approaching the whole-rock values of −5 to −11‰ measured in altered basalts from Krafla drillhole samples (Hattori and Muehlenbachs, 1982). The models that best match the observed $\delta^{18}O$ values for the domes are: andesitic crust at 3000 bars ($\delta^{18}O = -5‰$), hydrated basaltic crust at 2000 bars ($\delta^{18}O = -10‰$), amphibolite crust at 2000 or 3000 bars ($\delta^{18}O = -5‰$ and 0‰, respectively) and altered oceanic crust at 1000 bars ($\delta^{18}O = -5‰$) (Fig. 13B). Given the suggested average $\delta^{18}O$ value of −7‰ for the altered crust at Krafla (Hattori and Muehlenbachs, 1982), we suggest that models involving wallrock $\delta^{18}O$ of −5‰ (hydrated basaltic crust at 2000 bars, or altered oceanic crust at 1000 bars) represent the most realistic petrogenetic scenarios.

Although shallow (1000–2000 bars) AFC models involving wallrock $\delta^{18}O$ of −5‰ provide a good match to the isotopic compositions and are consistent with thermal modeling constraints, the bulk compositions of the final silicic magma produced do not reach the evolved rhyolitic compositions observed, and therefore require further differentiation outside of the thermal regime where assimilation of partial melt occurs (Figs. 12 and 13). The presence of zircons in the dome rhyolites provides additional thermal constraint; zircon crystallization occurs only when the temperature of the magma drops below the zircon saturation temperature (Boehnke et al., 2013; Loewen and Bindeman, 2015; Watson and Harrison, 1983), calculated at ~870–890 °C for the dome rhyolites (Boehnke et al., 2013; Watson and Harrison, 1983). In the simulated thermal system, this temperature threshold occurs >500 m from the main intrusion (Fig. 11C), suggesting that the magma must move out of this elevated temperature regime to sufficiently cool below zircon saturation (Fig. 11B and C). We thus suggest that more than one thermal environment is required to produce the rhyolitic dome magmas. The simple or complete lack of zircon zoning and lack of textural evidence for zircon resorption suggests that the magma was not reheated above the zircon saturation temperature after the onset of zircon grown, hence we infer that the dome zircons record the last stages of magmatic differentiation. One possible mechanism for achieving this substantial cooling is to remove the zircon undersaturated magma from the main area of heat along the fissure system to colder (and possibly shallower) areas of the crust where it can cool below zircon saturation. Such a scenario is consistent with the lack of systematic shifts in zircon $\delta^{18}O$ along the trace element fractional crystallization trends, which implies a lack of crustal assimilation during zircon fractionation and may reflect a cooler thermal environment.

In summary, our modeling results suggest that a two-step process is required to produce the Krafla rhyolite dome magmas (Fig. 14). First, partial melting of altered low $\delta^{18}O$ crust occurs in a relatively narrow zone around the margins of basaltic intrusions and is assimilated into the fractionating basaltic magma body (AFC). Second, the resulting low $\delta^{18}O$ dacitic melt is extracted and emplaced in cooler (and likely shallower) crust, where it undergoes additional fractional crystallization and cools below the zircon saturation temperature (Fig. 11). Similar two-step models have been suggested at other systems in Iceland (Martin and Sigmarsson, 2007) and at Yellowstone, where the low $\delta^{18}O$ signature of some rhyolites is imparted by incorporation of hydrothermally altered material (Troch et al., 2019; Troch et al., 2018) but

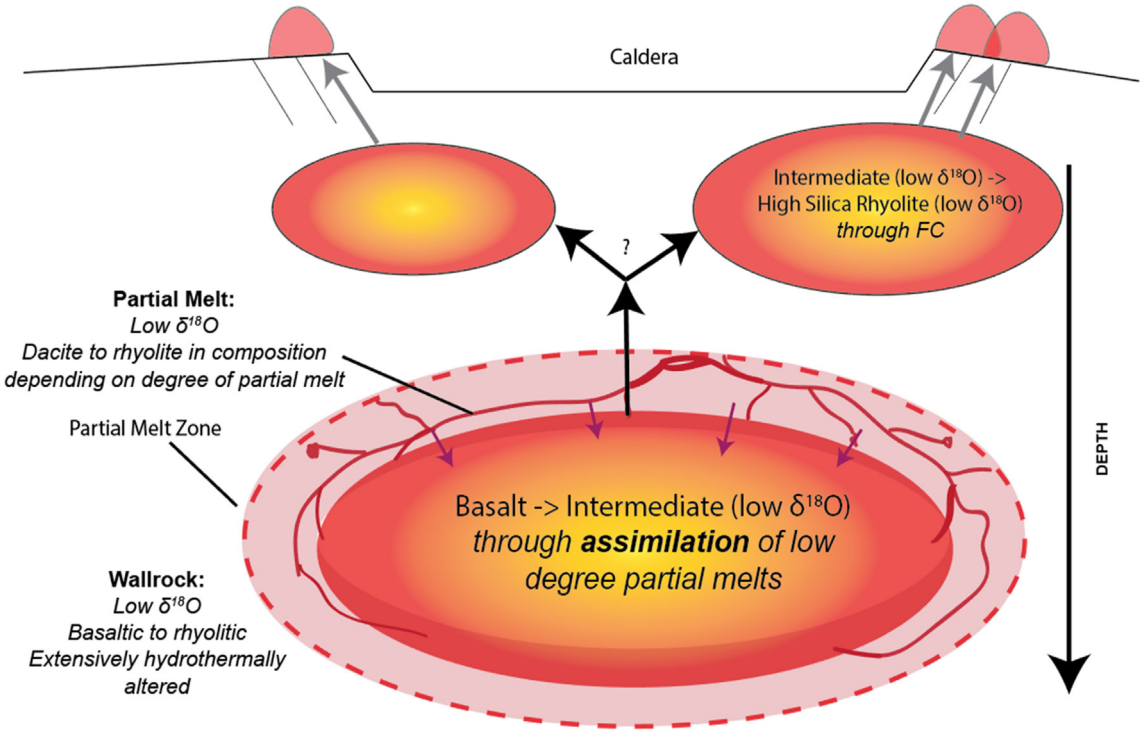

Fig. 14. New Model for Petrogenesis of the Rhyolite Domes. Schematic representation for the multi-stage petrogenetic model proposed for the three rhyolite domes. Low $\delta^{18}O$ partial melt from a compositionally diverse and isotopically depleted crust is assimilated after intrusion of mafic magma heats the surrounding crust. This imparts the low $\delta^{18}O$ signature and creates an intermediate to dacitic magma. Further differentiation to rhyolite occurs by fractional crystallization after removal of the magma to cooler crust where it cools below the zircon saturation temperature.

zircon crystallization occurs after removal from the zone where assimilation occurs (Loewen and Bindeman, 2015).

Our modeling results highlight the importance of hydrothermally altered crust in the differentiation of Krafla rhyolites. In the scenarios with dry crust, minimal partial melt is created, which means that differentiation must be driven by fractional crystallization (Fig. 12). This does not result in low $\delta^{18}O$ compositions. However, sufficient partial melt volumes can be generated to produce the observed isotopic characteristics (Fig. 13). The results of these numerical models are consistent with experimental data, which shows that the composition of the partial melt produced from altered mafic crust is predominantly dacitic, and that hydrothermally altered crust facilitates considerably more partial melt production at a given temperature (eg. Koepke et al., 2007; Koepke et al., 2005; Koepke et al., 2004; Spulber and Rutherford, 1982; Wolf and Wyllie, 1995).

Although our MCS models assume assimilation of partial melt rather than bulk crust, they cannot distinguish between bulk crustal assimilation versus assimilation of partial melt. Partial melting does not substantially alter the $\delta^{18}O$ signature of a material, hence both assimilation scenarios would lower the $\delta^{18}O$ of the magma in the same way. However, because of their high silica composition, assimilation of low-degree partial melts can assist in differentiating to higher silica compositions while simultaneously lowering the $\delta^{18}O$. In contrast, the magma composition can evolve substantially by bulk assimilation only if unerupted high silica material is assimilated. If the assimilant is basaltic, bulk assimilation is more (or entirely) reliant on fractional crystallization for differentiation. Such a scenario, while not specifically investigated in our models, provides a possible mechanism to produce low $\delta^{18}O$ basalts that have incorporated hydrothermally altered material but not evolved beyond their mafic compositions. Such processes may explain the occurrence of low $\delta^{18}O$ quartz-tholeiitic basalts with isotopically diverse crystal cargoes (Bindeman et al., 2008). To test this hypothesis, a detailed investigation of the trace element and whole rock chemistries in low $\delta^{18}O$ basalts in Iceland could be carried out to help reveal input from a more felsic partial melt or bulk crustal material.

4.3. Generation of other low $\delta^{18}O$ magmas at Krafla

Fig. 15 displays groundmass oxygen isotope values versus SiO_2 content for selected Krafla products spanning in age from pre-100 ka caldra to post caldera (Cooper et al., 2016; Nicholson et al., 1991). The basaltic end of this compositional spectrum has the greatest range in $\delta^{18}O$ values (~3‰ range, from +2.0 to +5.1‰) (Fig. 15), whereas higher silica compositions appear to cluster within a smaller range, overlapping with the lowest $\delta^{18}O$ values exhibited by the basaltic products (~2.5‰ range, from +1.0 to +3.5‰) (Fig. 15). Critically, all erupted lavas with SiO_2 greater than 53 wt% have groundmass $\delta^{18}O$ below +3.55‰ (Fig. 15). This suggests that lowering of magmatic $\delta^{18}O$ from mantle values of ~ + 5‰ occurs when the bulk magma composition is basaltic (<53 wt% SiO_2). Some significant $\delta^{18}O$ heterogeneity does appear in magmas with SiO_2 > 53 wt%, reflected by crystals found in the rhyolites (e.g., occasional high $\delta^{18}O$ pyroxenes). This may indicate at least some simultaneous assimilation and fractional crystallization through the intermediate stage of magma evolution, but the majority of differentiation to rhyolitic compositions appears to happen after the oxygen isotope signature has been imparted (Fig. 15). In this model, both normal and low $\delta^{18}O$ basalts (+2.0 to +5.0‰) can be erupted from the same system, dependent on the degree of crustal assimilation that they experience. This scenario is consistent with our two-step model for the petrogenesis of the dome rhyolites, which involves an early stage of differentiation involving assimilation of low $\delta^{18}O$ material followed by further FC without assimilation, and suggests that similar multi-step process may be common to many or most of the evolved magmas at Krafla. The near normal mantle values (+5 to +5.5‰) shown by some Krafla basalts (our analyses; Cooper et al., 2016; Nicholson et al., 1991) (Figs. 10 and 15), and the normal mantle-like olivine found in almost every low $\delta^{18}O$ basaltic lava in Iceland (Bindeman et al., 2008), imply that the low oxygen signature of many Icelandic magmas is more likely imparted primarily by incorporation of hydrothermally altered crust into relatively normal $\delta^{18}O$ magmas, rather than inherited from an anonymously low $\delta^{18}O$ plume signature, though there may certainly be some isotopic variability in the plume (e.g. Winpenny and Maclennan, 2014).

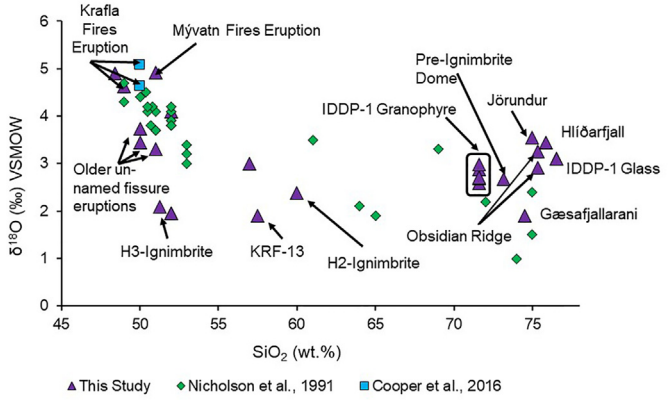

Fig. 15. $\delta^{18}O$ vs. SiO_2 $\delta^{18}O$ of glass or groundmass (this study) or bulk rock (Nicholson et al., 1991; Cooper et al., 2016) vs. SiO_2 for Krafla products.

5. Conclusions

Our combination of detailed isotopic analyses and thermal and chemical modeling provide important new insights into the generation of low $\delta^{18}O$ rhyolitic magmas at Krafla volcano, and represents a useful approach for exploring the petrogenesis of other enigmatic magmas. We show that the petrogenesis of Krafla rhyolites involves at least two-steps: 1) assimilation of hydrothermally altered material during fractional crystallization (AFC) to produce a low $\delta^{18}O$ intermediate to dacitic magma, followed by 2) further fractional crystallization with little to no concurrent assimilation to reach rhyolitic compositions.

Our models highlight the importance of hydrothermal alteration in the production of rhyolites at Krafla, and possibly in other areas of predominantly mafic crust. At Krafla, sustained basaltic intrusions accompanied by periodic glaciations during the early- to mid-Pleistocene thermally primed and hydrated the crust, producing a vigorous

hydrothermal system (Gautason and Muehlenbachs, 1998; Hattori and Muehlenbachs, 1982; Jónasson, 1994; Pope et al., 2013; Sæmundsson, 1991; Zakharov et al., 2019). This provided a fertile environment for rhyolite petrogenesis, allowing for more extensive crustal melting and assimilation to drive magmatic differentiation. To further understand this phenomenon, other systems with similar characteristics to Krafla can be tested using detailed oxygen isotope analyses and detailed modeling. These tools offer a method of investigating the interaction between intruding magmas and the crust in enigmatic systems and has a critical role to play in broadly interrogating volcanic plumbing systems.

CRediT authorship contribution statement

R.L. Hampton: Conceptualization, Methodology, Software, Formal analysis, Investigation, Data curation, Writing - original draft, Visualization, Funding acquisition. **I.N. Bindeman**: Conceptualization, Methodology, Supervision, Writing - review & editing, Resources. **R.A. Stern**: Formal analysis, Data curation, Writing - review & editing. **M.A. Coble**: Formal analysis, Data curation, Writing - review & editing. **S.M. Rooyakkers**: Validation, Data curation, Writing - review & editing, Resources, Conceptualization.

Declaration of Competing Interest

The authors declare that they have no known competing financial interests or personal relationships that could have appeared to influence the work reported in this paper.

Acknowledgements

We thank NSF 1822977 grant for support and RNF grant 19-17-00241 for zircon extraction and other support, University of Oregon and National Geographic society for travel support, David Zakharov for field and lab work assistance, Stanford-USGS facility for U-Th analyses, GSA Lipman fund for student analytical support. We also thank Catherine Annen who shared her Heat2D program modified by Dylan Colón for caldera-collapse situations. Michael Hudak was of great assistance during the modeling and both he and John Stix were of great help during the editing process.

Appendix A. Supplementary data

Supplementary data to this article can be found online at https://doi.org/10.1016/j.jvolgeores.2021.107229.

References

Annen, C., 2009. From plutons to magma chambers : thermal constraints on the accumulation of eruptible silicic magma in the upper crust. Earth Planet. Sci. Lett. 284, 409–416. https://doi.org/10.1016/j.epsl.2009.05.006.

Annen, C., Sparks, R.S.J., 2002. Effects of repetitive emplacement of basaltic intrusions on thermal evolution and melt generation in the crust. Earth Planet. Sci. Lett. 203, 937–955.

Axelsson, G., Egilson, T., Gylfadóttir, S.S., 2014. Modelling of temperature conditions near the bottom of well IDDP-1 in Krafla, Northeast Iceland. Geothermics, 49 https://doi.org/10.1016/j.geothermics.2013.05.003.

Banik, T.J., Miller, C.F., Fisher, C.M., Coble, M.A., Vervoort, J.D., 2018. Magmatic-tectonic control on the generation of silicic magmas in Iceland: Constraints from Hafnarfjall-Skarðsheiði volcano. Lithos 318–319, 326–339. https://doi.org/10.1016/j.lithos.2018.08.022.

Bindeman, I., 2008. Oxygen isotopes in mantle and crustal magmas as revealed by single crystal analysis. Rev. Mineral. Geochem. 69, 1–34. https://doi.org/10.2138/rmg.2008.69.11.

Bindeman, I.N., Melnik, O.E., 2016. Zircon survival, rebirth and recycling during crustal melting, magma crystallization, and mixing based on numerical modelling. J. Petrol. 57, 437–460. https://doi.org/10.1093/petrology/egw013.

Bindeman, I., Gurenko, A., Sigmarsson, O., Chaussidon, M., 2008. Oxygen isotope heterogeneity and disequilibria of olivine crystals in large volume Holocene basalts from Iceland: evidence for magmatic digestion and erosion of Pleistocene hyaloclastites. Geochim. Cosmochim. Acta 72, 4397–4420. https://doi.org/10.1016/j.gca.2008.06.010.

Bindeman, I., Gurenko, A., Carley, T., Miller, C., Martin, E., Sigmarsson, O., 2012. Silicic magma petrogenesis in Iceland by remelting of hydrothermally altered crust based on oxygen isotope diversity and disequilibria between zircon and magma with implications for MORB. Terra Nova 24, 227–232. https://doi.org/10.1111/j.1365-3121.2012.01058.x.

Boehnke, P., Watson, E.B., Trail, D., Harrison, T.M., Schmitt, A.K., 2013. Zircon saturation re-revisited. Chem. Geol. 351, 324–334. https://doi.org/10.1016/j.chemgeo.2013.05.028.

Bohrson, W.A., Spera, F.J., 2001. Energy-constrained open-system magmatic processes II: Application of energy-constrained assimilation fractional crystallization (EC-AFC) model to magmatic systems. J. Petrol. 42, 1019–1041.

Bohrson, W.A., Spera, F.J., Ghiorso, M.S., Brown, G.A., Creamer, J.B., Mayfield, A., 2014. Thermodynamic model for energy-constrained open-system evolution of crustal magma bodies undergoing simultaneous recharge, assimilation and crystallization: the magma chamber simulator. J. Petrol. https://doi.org/10.1093/petrology/egu036.

Calderone, G.M., Gronvold, K., Oskarsson, N., 1990. The welded air-fall tuff layer at Krafla, northern Iceland : a composite eruption triggered by injection of basaltic magma. J. Volcanol. Geotherm. Res. 44, 303–314.

Claiborne, L.L., Miller, C.F., Gualda, G.A.R., Carley, T.L., Covey, A.K., Wooden, J.L., Fleming, M.A., 2018. Zircon as Magma Monitor: Robust, Temperature-Dependent Partition Coefficients from Glass and Zircon Surface and Rim Measurements from Natural Systems. Microstruct. Geochronol. Planet. Rec. Down to Atom Scale. Geophys. Monogr. 232, 3–32.

Carley, T.L., Miller, C.F., Wooden, J.L., Bindeman, I.N., Barth, A.P., 2011. Zircon from historic eruptions in Iceland: Reconstructing storage and evolution of silicic magmas. Mineral. Petrol. 102, 135–161. https://doi.org/10.1007/s00710-011-0169-3.

Carley, T.L., Miller, C.F., Wooden, J.L., Padilla, A.J., Schmitt, A.K., Economos, R.C., Bindeman, I.N., Jordan, B.T., 2014. Iceland is not a magmatic analog for the Hadean: evidence from the zircon record. Earth Planet. Sci. Lett. 405, 85–97. https://doi.org/10.1016/j.epsl.2014.08.015.

Carley, T.L., Miller, C.F., Fisher, C.M., Hanchar, J.M., Vervoort, J.D., Schmitt, A.K., Economos, R.C., Jordan, B.T., Padilla, A.J., Banik, T.J., 2020. Petrogenesis of silicic magmas in Iceland through space and time: the isotopic record preserved in zircon and whole rocks. J. Geol. 128, 1–28. https://doi.org/10.1086/706261.

Carmichael, I., 1964. The petrology of Thingmuli, a Tertiary volcano in eastern Iceland. J. Petrol. 5, 435–460.

Cashman, K.V., Marsh, B.D., 1988. Crystal size distribution (CSD) in rocks and the kinetics and dynamics of crystallization - II. Makaopuhi lava lake. Contrib. Mineral. Petrol. 99, 292–305. https://doi.org/10.1007/BF00371933.

Charreteur, G., Tegner, C., Haase, K., 2013. Multiple ways of producing intermediate and silicic rocks within Thingmúli and other Icelandic volcanoes. Contrib. Mineral. Petrol. 166, 471–490. https://doi.org/10.1007/s00410-013-0886-1.

Coble, M.A., Vazquez, J.A., Barth, A.P., Wooden, J., Burns, D., Kylander-clark, A., Jackson, S., Vennari, C.E., 2018. Trace element characterisation of MAD-559 zircon reference material for ion microprobe analysis. Geostand. Geoanal. Res. https://doi.org/10.1111/ggr.12238.

Cooper, K.M., Sims, K.W.W., Eiler, J.M., Banerjee, N., 2016. Timescales of storage and recycling of crystal mush at Krafla Volcano, Iceland. Contrib. Mineral. Petrol. 171, 1–19. https://doi.org/10.1007/s00410-016-1267-3.

Eichelberger, J., 2020. Distribution and transport of thermal energy within magma–hydrothermal systems. Geosci. 10, 1–26. https://doi.org/10.3390/geosciences10060212.

Eichelberger, J., Kiryukhin, A., Mollo, S., Tsuchiya, N., Villeneuve, M., 2020. Exploring and modeling the magma–hydrothermal regime. Geosci. 10, 1–6. https://doi.org/10.3390/geosciences10060234.

Einarsson, P., 1978. S-wave shadows in the Krafla Caldera in NE-Iceland, evidence for a magma chamber in the crust. Bull. Volcanol. 41, 187–195. https://doi.org/10.1007/BF02597222.

Einarsson, P., Brandsdóttir, B., 1980. Seismological evidence for lateral magma intrusion during the July 1978 deflation of the Krafla volcano in NE- Iceland. J. Geophys. 47, 160–165. https://doi.org/10.2172/890964.

Elders, W.A., Fridleifsson, G.Ó., Zierenberg, R.A., Pope, E.C., Mortensen, A.K., Gudmundsson, Á., Lowenstern, J.B., Marks, N.E., Owens, L., Bird, D.K., Reed, M., Olsen, N.J., Schiffman, P., 2011. Origin of a rhyolite that intruded a geothermal well while drilling at the Krafla volcano, Iceland. Geology 39, 231–234. https://doi.org/10.1130/G31393.1.

Elders, W.A., Frioleifsson, G.O., Albertsson, A., 2014. Drilling into magma and the implications of the Iceland Deep Drilling Project (IDDP) for high-temperature geothermal systems worldwide. Geothermics 49, 111–118. https://doi.org/10.1016/j.geothermics.2013.05.001.

Furman, T., Frey, F.A., Meyer, P.S., 1992. Petrogenesis of evolved basalts and rhyolites at austurhorn, southeastern Iceland: the role of fractional crystallization. J. Petrol. 33, 1405–1445. https://doi.org/10.1093/petrology/33.6.1405.

Gautason, B., Muehlenbachs, K., 1998. Oxygen isotopic fluxes associated with high-temperature processes in the rift zones of Iceland. Chem. Geol. 145, 275–286.

GERM, 2015. Geochemical earth reference model partition coefficient (Kd) database [WWW Document]. Earth Ref. http://earthref.org/KDD/

Ghiorso, M.S., Sack, R., 1995. Chemical mass transfer in magmatic processes IV. Contrib. Mineral. Petrol. 119, 197–212. https://doi.org/10.1007/BF00307281.

Grönvold, K., 1984. Myvatn Fires 1724-1729; Chemical Composition of the Lava. Nord. Volcanol. Institute, Reyjavik. 1 pp. 1–31.

Gurenko, A.A., Bindeman, I.N., Sigurdsson, I.A., 2015. To the origin of Icelandic rhyolites: insights from partially melted leucocratic xenoliths. Contrib. Mineral. Petrol. 169, 1–21. https://doi.org/10.1007/s00410-015-1145-4.

Hards, V., Kempton, P., Thompson, R., Greenwood, P., 2000. The magmatic evolution of the Snæfell volcanic Centre; an example of volcanism during incipient rifting in Iceland. J. Volcanol. Geotherm. Res. 99, 97–121.

Hattori, K., Muehlenbachs, K., 1982. Oxygen isotope ratios of the Icelandic crust. J. Geophys. Res. 87, 6559–6565.
Hjartardóttir, A.R., Einarsson, P., Magnúsdóttir, S., Björnsdóttir, T., Brandsdóttir, B., 2016. Fracture systems of the Northern Volcanic Rift Zone, Iceland: an onshore part of the Mid-Atlantic plate boundary. Geol. Soc. Spec. Publ. 420, 297–314. https://doi.org/10.1144/SP420.1.
Hoefs, J., 2015. Stable Isotope Geochemistry. 6th ed. Springer International Publishing, Switzerland.
Jónasson, K., 1994. Rhyolite volcanism in the Krafla central volcano, north-East Iceland. Bull. Volcanol. 56, 516–528. https://doi.org/10.1007/BF00302832.
Jónasson, K., 2007. Silicic volcanism in Iceland : Composition and distribution within the active volcanic zones. J. Geodyn. 43, 101–117. https://doi.org/10.1016/j.jog.2006.09.004.
Kennedy, B.M., Holohan, E.P., Stix, J., Gravley, D.M., Davidson, J.R.J., Cole, J.W., 2018. Magma plumbing beneath collapse caldera volcanic systems. Earth-Sci. Rev. 177, 404–424. https://doi.org/10.1016/j.earscirev.2017.12.002.
Koepke, J., Feig, S.T., Snow, J., Freise, M., 2004. Petrogenesis of oceanic plagiogranites by partial melting of gabbros: an experimental study. Contrib. Mineral. Petrol. 146, 414–432. https://doi.org/10.1007/s00410-003-0511-9.
Koepke, J., Feig, S.T., Snow, J., 2005. Hydrous partial melting within the lower oceanic crust. Terra Nova 17, 286–291. https://doi.org/10.1111/j.1365-3121.2005.00613.x.
Koepke, J., Berndt, J., Feig, S., Holtz, F., 2007. The formation of SiO 2 -rich melts within the deep oceanic crust by hydrous partial melting of gabbros. Contrib. Mineral. Petrol., 67–84 https://doi.org/10.1007/s00410-006-0135-y.
Kokfelt, T., Hoernle, K., Lundstrom, C., Hauff, F., Bogaard, C., 2009. Time-scales for magmatic differentiation at the Snaefellsjo central volcano, western Iceland : Constraints from U – Th – Pa – Ra disequilibria in post-glacial lavas. Geochim. Cosmochim. Acta 73, 1120–1144. https://doi.org/10.1016/j.gca.2008.11.021.
Kuo, T., 2017. The Composition of Altered Oceanic Crust: Implications for Mantle Evolution (Dissertation). University of Melbourne.
Loewen, M.W., Bindeman, I.N., 2015. Oxygen isotope and trace element evidence for three-stage petrogenesis of the youngest episode (260–79 ka) of Yellowstone rhyolitic volcanism. Contrib. Mineral. Petrol. 170, 1–25. https://doi.org/10.1007/s00410-015-1189-5.
Maas, R., Kinny, P.D., Williams, I.S., Froude, D.O., Compston, W., 1992. The Earth's oldest known crust: a geochronological and geochemical study of 3900-4200 Ma old detrital zircons from Mt. Narryer and Jack Hills, Western Australia. Geochim. Cosmochim. Acta 56, 1281–1300. https://doi.org/10.1016/0016-7037(92)90062-N.
Macdonald, R., McGarvie, D., Pinkerton, H., Smith, R., Palacz, A., 1990. Petrogenetic evolution of the Torfajökull volcanic complex, Iceland I. Relationship between the magma types. J. Petrol. 31, 429–459.
Maclennan, J., Jull, M., McKenzie, D., Slater, L., Grönvold, K., 2002. The link between volcanism and deglaciation in iceland. Geochem. Geophys. Geosyst. 3, 1–25. https://doi.org/10.1029/2001GC000282.
Marsh, B.D., 1988. Crystal size distribution (CSD) in rocks and the kinetics and dynamics of crystallization - I. Theory. Contrib. Mineral. Petrol. 99, 277–291. https://doi.org/10.1007/BF00371933.
Marsh, B.D., 2007. Crystallization of silicate magmas deciphered using crystal size distributions. J. Am. Ceram. Soc. 90, 746–757 https://doi.org/10.1111/j.1551-2916.2006.01473.x.
Marsh, B.D., Gunnarsson, B., Congdon, R., Carmody, R., 1991. Hawaiian basalt and Icelandic rhyolite: Indicators of differentiation and partial melting. Geol. Rundsch. 80, 481–510. https://doi.org/10.1007/BF01829378.
Martin, E., Sigmarsson, O., 2007. Crustal thermal state and origin of silicic magma in Iceland: the case of Torfajökull, Ljósufjöll and Snæfellsjökull volcanoes. Contrib. Mineral. Petrol. 153, 593–605. https://doi.org/10.1007/s00410-006-0165-5.
Martin, E., Sigmarsson, O., 2010. Thirteen million years of silicic magma production in Iceland: Links between petrogenesis and tectonic settings. Lithos 116, 129–144. https://doi.org/10.1016/j.lithos.2010.01.005.
Martin, E., Martin, H., Sigmarsson, O., 2008. Could Iceland be a modern analogue for the Earth's early continental crust? Terra Nova 20, 463–468. https://doi.org/10.1111/j.1365-3121.2008.00839.x.
Melnik, O., Bindeman, I., 2018. Modeling of trace elemental zoning patterns in accessory minerals with emphasis on the origin of micrometer-scale oscillatory zoning in zircon. Am. Minerol. https://doi.org/10.2138/am-2018-6182.
Mucek, A.E., Danis, M., De Silva, S.L., Schmitt, A.K., Pratomo, I., Coble, M.A., 2017. Post-supereruption recovery at Toba Caldera. Nat. Commun. 1–9. https://doi.org/10.1038/ncomms15248.
Nicholson, H., 1990. The Magmatic Evolution of Krafla, NE Iceland (Dissertation). University of Edinburgh.
Nicholson, H., Latin, D., 1992. Olivine tholeiites from krafla, Iceland: evidence for variations in melt fraction within a plume. J. Petrol. 33, 1105–1124. https://doi.org/10.1093/petrology/33.5.1105.
Nicholson, H., Condomines, M., Fitton, J.G., Fallick, A., Gronvold, K., Rogers, G., 1991. Geochemical and isotopic evidence for crustal assimilation beneath Krafla, Iceland. J. Petrol. 32, 1005–1020.
Pope, E.C., Bird, D.K., Arnórsson, S., 2013. Evolution of low-18O Icelandic crust. Earth Planet. Sci. Lett. 374, 47–59. https://doi.org/10.1016/j.epsl.2013.04.043.
Pope, E.C., Bird, D.K., Arnórsson, S., 2014. Stable isotopes of hydrothermal minerals as tracers for geothermal fluids in Iceland. Geothermics 49, 99–110. https://doi.org/10.1016/j.geothermics.2013.05.005.
Reimink, J.R., Chacko, T., Stern, R.A., Heaman, L.M., 2014. Earth's earliest evolved crust generated in an Iceland-like setting. Nat. Geosci. 7, 529–533. https://doi.org/10.1038/ngeo2170.
Rooyakkers, S.M., 2020. New Insights on Rhyolitic and Mixed Rhyolitic-Basaltic Magmatism and Volcanism at Krafla Central Volcano, Iceland (Dissertation). McGill University.
Rooyakkers, S.M., Stix, J., Berlo, K., Barker, S.J., 2020. Emplacement of unusual rhyolitic to basaltic ignimbrites during collapse of a basalt-dominated caldera: the Halarauður eruption, Krafla (Iceland). GSA Bull. 132, 1881–1902. https://doi.org/10.1130/b35450.1.
Rooyakkers, S.M., Stix, J., Berlo, K., Petrelli, M., Hampton, R., 2021. In Review, The origin of rhyolitic magmatism at Krafla Central Volcano (Iceland). J. Petrol.
Sæmundsson, K., 1991. Jarðfræði Kröflukerfisins (the geology of the Krafla volcanic system, in Icelandic). Náttúra Mývatns 3–60.
Sæmundsson, K., Pringle, M.S., 2000. Um aldur berglaga Í Kröflukerfinu (On the age of rock strata in the Krafla system). Geosci. Soc. Icel. Spring Meet. Abstr. Reykjavík, Iceland, Geosci. Soc. Icel, pp. 26–27.
Schattel, N., Portnyagin, M., Golowin, R., Hoernle, K., Bindeman, I., 2014. Contrasting conditions of rift and off-rift silicic magma origin on Iceland. Geophys. Res. Lett. 41, 5813–5820. https://doi.org/10.1002/2014GL060780.
Sigmarsson, O., Steinthórsson, S., 2007. Origin of Icelandic basalts : a review of their petrology and geochemistry. J. Geodyn. 43, 87–100. https://doi.org/10.1016/j.jog.2006.09.016.
Simakin, A.G., Bindeman, I.N., 2008. Evolution of crystal sizes in the series of dissolution and precipitation events in open magma systems. J. Volcanol. Geotherm. Res. 177, 997–1010. https://doi.org/10.1016/j.jvolgeores.2008.07.012.
Spulber, D., Rutherford, M.J., 1982. The origin of rhyolite and plagiogranite in oceanic crust: an experimental study. J. Petrol. 24, 1–25.
Sveinbjornsdóttir, Á.E., Ármannsson, H., Óskarsson, F., Ólafsson, M., 2015. A conceptual hydrological model of the thermal areas within the northern neovolcanic zone, Iceland using stable water isotopes. Proc. World Geotherm. Congr. 19–25.
Thorarinsson, S., 1979. The postglacial history of the Mývatn area. Nord. Soc. Oikos 32, 16–28.
Troch, J., Ellis, B.S., Schmitt, A.K., Bouvier, A.S., Bachmann, O., 2018. The dark side of zircon: textural, age, oxygen isotopic and trace element evidence of fluid saturation in the subvolcanic reservoir of the Island Park-Mount Jackson Rhyolite, Yellowstone (USA). Contrib. Mineral. Petrol. 173, 1–17. https://doi.org/10.1007/s00410-018-1481-2.
Troch, J., Ellis, B.S., Harris, C., Ulmer, P., Bouvier, A.-S., Bachmann, O., 2019. Experimental melting of hydrothermally altered rocks: constraints for the generation of low δ18O rhyolites in the Central Snake River Plain. J. Petrol. 60, 1881–1902. https://doi.org/10.1093/petrology/egz056.
Tuffen, H., Castro, J.M., 2009. The emplacement of an obsidian dyke through thin ice: Hrafntinnuhryggur, Krafla Iceland. J. Volcanol. Geotherm. Res. 185, 352–366. https://doi.org/10.1016/j.jvolgeores.2008.10.021.
Valley, J.W., Chiarenzelli, J.R., McLelland, J.M., 1994. Oxygen isotope geochemistry of zircon. Earth Planet. Sci. Lett. 126, 187–206.
Watson, E.B., Harrison, T.M., 1983. Zircon saturation revisited: temperature and composition effects in a variety of crustal magma types. Earth Planet. Sci. Lett. 64, 295–304.
Weisenberger, T.B., Axelsson, G., Arnaldsson, A., Blischke, A., Óskarsson, F., Ármannsson, H., Blanck, H., Helgadóttir, H.M., Berthet, J.C., Árnason, K., Ágústsson, K., Gylfadóttir, S.S., Guðmundsdóttir, V., 2015. Revision of the Conceptual Model of the Krafla Geothermal System (Landsvirkjun).
Winpenny, B., Maclennan, A.J., 2014. Short length scale oxygen isotope heterogeneity in the icelandic mantle: evidence from plagioclase compositional zones. J. Petrol. 55, 2537–2566. https://doi.org/10.1093/petrology/egu066.
Wolf, B., Wyllie, J., 1995. Liquid segregation parameters from amphibolite dehydration melting experiments. J. Geophys. Res. 100, 15611–15621.
Zakharov, D.O., Bindeman, I., Tanaka, R., Friðleifsson, G., Reed, M., Hampton, R., 2019. Triple oxygen isotope systematics as a tracer of fluids in the crust: a study from modern geothermal systems of Iceland. Chem. Geol. 530, 1–13. https://doi.org/10.1016/j.jenvman.2020.110644.
Zierenberg, R.A., Schiffman, P., Barfod, G.H., Lesher, C.E., Marks, N.E., Lowenstern, J.B., Mortensen, A.K., Pope, E.C., Bird, D.K., Reed, M.H., Fridleifsson, G.Ó., Elders, W.A., 2013. Composition and origin of rhyolite melt intersected by drilling in the Krafla geothermal field, Iceland. Contrib. Mineral. Petrol. 165. https://doi.org/10.1007/s00410-012-0811-z.